



Biomechanics of the mandible of *Macaca mulatta* during the power stroke of mastication: Loading, deformation, and strain regimes and the impact of food type

Olga Panagiotopoulou^{a,*}, Jose Iriarte-Diaz^b, Hyab Mehari Abraha^a, Andrea B. Taylor^c, Simon Wilshin^d, Paul C. Dechow^e, Callum F. Ross^{f,*}

^a Department of Anatomy & Developmental Biology, Monash Biomedicine Discovery Institute, Faculty of Medicine Nursing and Health Sciences, Monash University, Clayton, Melbourne, Victoria, 3800, Australia

^b Department of Biology, University of the South, Sewanee, TN, 37383, USA

^c Department of Basic Science, Touro University, CA, USA

^d Comparative Biomedical Sciences, The Royal Veterinary College, Hawkshead Lane, Herts, AL97TA, UK

^e Department of Biomedical Sciences, Texas A&M University College of Dentistry, Dallas, TX, USA

^f Department of Organismal Biology and Anatomy, University of Chicago, Chicago, IL, 60637, USA

ARTICLE INFO

Article history:

Received 28 March 2020

Accepted 21 July 2020

Available online 6 September 2020

Keywords:

Chewing

Feeding

Electromyography

Strain

Finite element modeling (FEM)

ABSTRACT

Mandible morphology has yet to yield definitive information on primate diet, probably because of poor understanding of mandibular loading and strain regimes, and overreliance on simple beam models of mandibular mechanics. We used a finite element model of a macaque mandible to test hypotheses about mandibular loading and strain regimes and relate variation in muscle activity during chewing on different foods to variation in strain regimes. The balancing-side corpus is loaded primarily by sagittal shear forces and sagittal bending moments. On the working side, sagittal bending moments, anteroposterior twisting moments, and lateral transverse bending moments all reach similar maxima below the bite point; sagittal shear is the dominant loading regime behind the bite point; and the corpus is twisted such that the mandibular base is inverted. In the symphyseal region, the predominant loading regimes are lateral transverse bending and negative twisting about a mediolateral axis. Compared with grape and dried fruit chewing, nut chewing is associated with larger sagittal and transverse bending moments acting on balancing- and working-side mandibles, larger sagittal shear on the working side, and larger twisting moments about vertical and transverse axes in the symphyseal region. Nut chewing is also associated with higher minimum principal strain magnitudes in the balancing-side posterior ramus; higher sagittal shear strain magnitudes in the working-side buccal alveolar process and the balancing-side oblique line, recessus mandibulae, and endocondylar ridge; and higher transverse shear strains in the symphyseal region, the balancing-side medial prominence, and the balancing-side endocondylar ridge. The largest food-related differences in maximum principal and transverse shear strain magnitudes are in the transverse tori and in the balancing-side medial prominence, extramolar sulcus, oblique line, and endocondylar ridge. Food effects on the strain regime are most salient in areas not traditionally investigated, suggesting that studies seeking dietary effects on mandible morphology might be looking in the wrong places.

© 2020 Elsevier Ltd. All rights reserved.

1. Introduction

“Strain gauges suffer from the limitation that they cannot sample the total strain environment. This is probably an intractable problem. On the other hand, lack of knowledge of biological parameters (masticatory force vectors and mandibular material properties) currently constrains finite element

* Corresponding authors.

E-mail addresses: olga.panagiotopoulou@monash.edu (O. Panagiotopoulou), rossc@uchicago.edu (C.F. Ross).

work; this problem may not be insoluble, but it is unlikely to be resolved in the near future. The errors in finite element models are not known, and a first step toward their assessment could be achieved by validating models with experimental strain data” (Daegling and Hylander, 2000: 549).

Despite decades of research into the relationship between the morphology and function of the hominid cranium, fundamental aspects of fossil hominid diet (what they ate) and feeding behavior (how they ate) remain unresolved (Grine et al., 2010; Ledogar et al., 2016; Rak, 1983; Robinson, 1972; Scott et al., 2005; Smith et al., 2015b; Spears and Macho, 1998; Strait et al., 2009, 2013; Ungar et al., 2008). This is probably due, in part, to the fact that the cranium performs a variety of functions, making it difficult to identify signals of feeding adaptations that are unaffected by selection for other functions, such as orienting, housing, and protecting eyes, ears, and brains (Hylander et al., 1991; Lieberman et al., 2000; Ross et al., 2011; Ross and Iriarte-Díaz, 2014). As mandibles perform a narrower range of functions than the cranium, their morphology might display stronger covariation with diet and feeding behavior.

Current models of anthropoid primate mandible mechanics are based in large part on in vivo studies in macaques by W.L. Hylander in which hypotheses about mandibular stress, strain, and deformation regimes (sensu Ross et al., 2011) were derived from in vivo bone strain data from small areas of the corpus and symphysis (Hylander, 1977, 1979a, b, c, 1981, 1984, 1985, 1986, 1988; Hylander et al., 1987). In these studies, the in vivo data were explained and interpreted using simple beam models and assumptions about the relative magnitudes and orientations of the forces acting on the mandible during feeding. Subsequent studies then deployed the model to motivate morphometric studies of interspecific and intraspecific variation in primate mandible form (Daegling, 1989, 1993, 2007a, b; Daegling and Grine, 1991, 2006; Daegling and Hotzman, 2003; Daegling and Hylander, 1998, 2000; Daegling et al., 1992; Dechow and Hylander, 2000; Demes et al., 1984; Hylander, 1979b, c, 1984, 1985, 1988; Ravosa, 1991, 1996a, b, 1999, 2000; Ravosa and Hogue, 2004; Ravosa and Simons, 1994; Ravosa et al., 2000; Taylor, 2002, 2005, 2006a, b; Taylor et al., 2008; Vogel et al., 2014; Wolff, 1984). This intensive comparative morphometric research has yet to uncover strong relationships between mandible form, feeding behavior, and diet in living primates (Daegling, 2007b; Daegling et al., 2016; Daegling and Grine, 2006; Hylander, 1988; McGraw and Daegling, 2012, 2020; Ravosa et al., 2016; Ross and Iriarte-Díaz, 2019; Taylor, 2002, 2006a).

Several reasons for lack of a clear-cut relationship between mandibular morphology, feeding behavior, and diet have been suggested (Daegling and Hylander, 2000; Ross and Iriarte-Díaz, 2014, 2019; Ross et al., 2012; Taylor et al., 2008). One possibility is that simple beam models do not capture the complexity of mandibular strain regimes accurately enough and that more realistic models would suggest that different kinds of measurements are needed, maybe in different places. The limitations of simple beam models—prismatic structure and homogeneous material properties—are widely acknowledged (Chalk et al., 2011; Daegling, 1993; Daegling and Hylander, 1998, 2000). The best method for overcoming these limitations is finite element modeling (FEM) wherein geometry and material properties can be represented more precisely than in a simple beam and the sensitivity of the model to their errors and variation can be quantified (Daegling and Hylander, 2000; Gróning et al., 2012; Moazen et al., 2009; Panagiotopoulou et al., 2017; Porro et al., 2011, 2013; Rayfield, 2011; Smith et al., 2015a, b; Strait et al., 2005, 2007, 2009, 2010; Wroe et al., 2007). Moreover, FEM makes it possible to estimate strain regimes throughout the mandible, not just in the small areas

historically sampled by strain gauges, and to estimate all of the components of the strain regime—shear and principal strains.

Our understanding of primate mandible design—form-function relationships—might also be improved by better understanding of variation in external forces associated with different feeding behaviors and the impact of those loading regimes on mandibular strain regimes. For example, increased consumption of “tougher and more fibrous foods” (Hylander, 1979c: 294, 1985: 328) requires “recruitment of relatively greater amounts of balancing-side muscle force” (Hylander, 1985: 328–329), and this is hypothesized to require increased symphyseal strength to counter increased symphyseal stresses (Hylander, 1979c, 1985; Ravosa, 1996a, b, 2000). However, the exact nature of those stresses is not known. Increases in vertical components of balancing-side muscle force would increase frontal shear stresses, whereas increases in transverse components would increase transverse bending—‘wishboning’—stresses. However, all jaw muscles generate forces with both vertical and transverse components, and the relative magnitudes of the associated moments can vary with changes in muscle activation and relaxation through the gape cycle (Hylander and Johnson, 1989, 1993, 1994; Hylander et al., 1987, 2000, 2002, 2004, 2005, 2011). Consequently, the effects of this force modulation on mandibular strain regimes are difficult to estimate with much precision. FEM is also currently the best solution to this problem. Mandibular loading regimes can be precisely modeled using estimates of muscle forces based on electromyographic (EMG) and muscle architecture data, enabling more accurate and precise estimates of relative muscle force (Panagiotopoulou et al., 2017; Weijs and Dantuma, 1975, 1981; Weijs and Van der Wielen-Drent, 1982). When these data are combined with accurate measures of muscle attachment locations and orientations, it is possible to make precise—and hopefully accurate—estimates of moments and shearing forces, enabling testing of hypotheses about mandibular loading regimes.

These advantages of FEM led us to develop a finite element model of the mandible of an adult female rhesus monkey (*Macaca mulatta*; Panagiotopoulou et al., 2017). The geometry of the model was based on computed tomography scans of the animal's mandible, bone material properties were measured from the specimen postmortem (Dechow et al., 2017; Panagiotopoulou et al., 2017), and external forces were estimated using a combination of in vivo EMG and muscle architecture data collected from the same individual. The model was validated against in vivo strain gauge data recorded when the animal was chewing on three different food types: nuts, dried fruits, and grapes (Mehari Abraha et al., 2019; Panagiotopoulou et al., 2017).

Here, we deploy this model to address three questions. First, we ask whether the loading regime of our FEM—the combination of external forces acting on the mandible—and the FEM deformation regime—the overall pattern of deformation—match current ideas about anthropoid mandible mechanics during the power stroke of mastication (Demes et al., 1984; Hylander, 1979b, c, 1984, 1985, 1988; Hylander et al., 1987; van Eijden, 2000; Wolff, 1984).

Second, we ask what mandibular strain regime is associated with these loading and deformation regimes. Previous research has focused on strain regimes in the areas where strains have been recorded in vivo, especially the lateral prominence of the corpus and the labial surface of the symphysis, and made assumptions about patterns of strain in other areas. Here, we provide a more comprehensive description of strain regimes throughout the macaque mandible, including principal, axial, and shear strains. This description contextualizes our discussion of food-related variation in strain regimes, provides novel insights into mandible mechanics during chewing, and suggests new hypotheses about mandible form-function relationships. This description also lays the

groundwork for FEM analyses of hominid primate mandibles currently in preparation.

Finally, we ask how variation in loading regimes associated with mastication on foods of different material properties affects deformation and strain regimes in the mandible. Specifically, we ask which areas of the mandible are most affected by variation in the loading regime associated with variation in food material properties and which strain components vary the most. These results are important for researchers interested in hominid evolution because they provide insight into the ability of traditional measures of mandible form—corpus and symphyseal external dimensions—to identify differences in feeding behavior or diet in extinct primates and because they suggest new aspects of morphology for comparative and evolutionary analysis.

Terminology of mandible morphology and coordinate systems used to describe mandible morphology and loading, deformation, and strain regimes is given in Figure 1. The ramus is the mandible posterior to M₃ and includes the coronoid and condylar processes; the corpus of the mandible extends from below M₃ to a frontal

plane through the back of the midline symphyseal region, roughly level with the P₃s; the symphyseal region lies between the P₃s on each side. Inner and outer surfaces of the ramus are referred to as medial and lateral, of the corpus as lingual and buccal, and of the symphyseal region as lingual and labial. In transverse planes (seen from superior and inferior views), the V-shaped basal arch of the mandibular corpora converges on the symphyseal region more sharply and more posteriorly than the U-shaped arch of the alveolar processes (Virchow, 1916, 1920; Weidenreich, 1936). Superiorly, this exposes a chevron-shaped planum alveolare, which is broad in the symphyseal region—lingual to the incisors, canines, and P₃s—and tapers posteriorly into the alveolar process of the M₂ on each side. Where the V-shaped outline of the basal mandibular arch diverges posteriorly to grade into the rami, the alveolar processes of the M₃ and the retromolar trigon curve lingually to form an alveolar prominence (prominentia alveolaris; Weidenreich, 1936) protruding over the submandibular fossa. Anteriorly, this alveolar prominence is connected to the superior transverse torus of the symphyseal region by a variably developed and variably

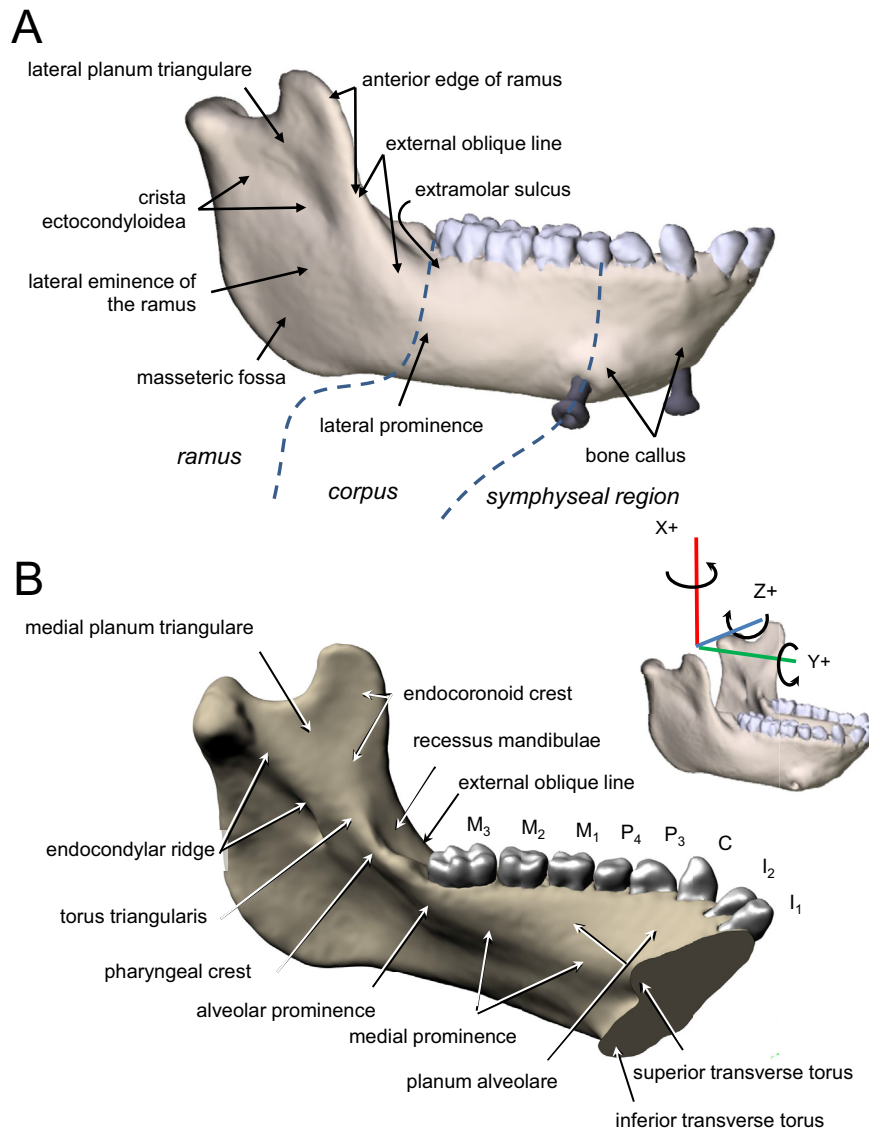


Figure 1. A, B) Terminology used in this paper. C, D) Coordinate system and conventions for strain and deformation regimes. Abbreviations: AP = anteroposterior; SI = superoinferior.

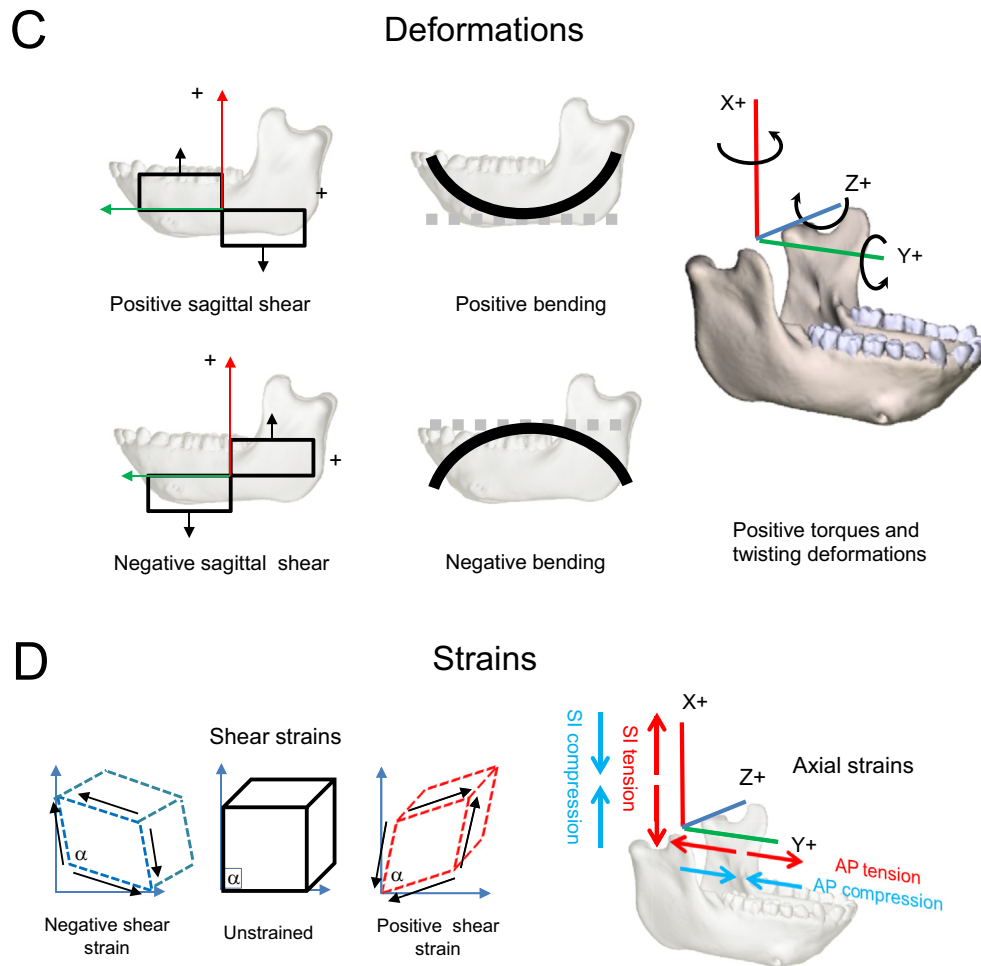


Figure 1. (continued).

named ridge of bone: in *Homo*, this has been referred to as a “slight bony ridge” (Gaspard, 1978: Fig. 61), as an “alveolar prominence” sensu lato (Rightmire and Deacon, 1991; Weidenreich, 1936: 47), or perhaps as “torus alveolaris” (Weidenreich, 1936: 99). We suggest that alveolar prominence should be reserved for the posterior extremity of the medial prominence, in part because using that term to refer to the entire ridge of bone running anteriorly from the alveolar prominence sensu stricto gives the erroneous impression that the ridge is structurally, functionally, or developmentally part of the alveolar process. We instead use the term medial prominence of the corpus, or simply medial prominence, to refer to the ridge of bone connecting the superior transverse torus of the symphyseal region with the alveolar prominence at the back end of the tooth row. Together, these three structures form the lingual outline of the upper mandibular corpus and symphysis, Virchow’s arcus intermedius, and Weidenreich’s inner mandibular arch (Virchow, 1920; Weidenreich, 1936).

The mylohyoid line is distinct from the medial prominence, although the line crosses the prominence in its course from the ramus to the symphyseal region. When it is well defined, the mylohyoid line extends from the inferior transverse torus to the ramus below (and, sometimes in humans, at) the torus triangularis. As it crosses the alveolar prominence, the mylohyoid line angles anteroinferiorly, leaving room for the lingual nerve to enter the floor of the mouth between the medial edge of the posterior alveolus and the mylohyoid muscle. The internal oblique line of dental radiology corresponds to the mylohyoid line (and sometimes

torus triangularis). A variably robust ridge of bone extending posteriorly from the alveolar prominence to the condylar neck is divided into, from front to back, the crista pharyngea, torus triangularis, and endocondylar crest (Gaspard, 1978; Piveteau, 1957; Weidenreich, 1936) or endocondylar ridge (White et al., 2012). An endocoronoid crest diverges from torus triangularis and extends superiorly toward the tip of the coronoid process. Anterior to the endocoronoid crest, the front edge of the ramus is marked by the temporal crest, which splits to enclose a shallow recessus mandibulae (Lenhossek, 1920), which in turn opens inferiorly into the extramolar sulcus (Keiter, 1935). Lateral to this sulcus, the anterior edge of the ramus continues down onto the buccal corpus as the external oblique line of the mandible, which merges with the lateral prominence (Rasche, 1913) below M_3 .

Definitions of terms used to describe loading, deformation, and strain regimes follow Ross et al. (2011). The loading regime is the combination of external forces acting on the mandible, in vivo or in silico. Loading regimes are summarized here as shear forces and twisting moments or torques. Stress and strain regimes are the patterns of internal forces and strains within the mandible or FEM associated with a given loading regime. Here, the strain regimes are the axial, principal, and shear strains in the surface of the model. Deformation regimes are the patterns of deformation of the mandible—the integral of the strain regime across the mandible—associated with the loading regimes. Here, the deformation regimes are bending, shearing, and twisting within and about specified axes and planes.

To facilitate comparisons with the prior literature, loading, strain, and deformation regimes are described in an anatomical coordinate system aligned with a right-handed Cartesian coordinate system. The X-axis is superoinferior (SI); the Y-axis is anteroposterior (AP); the Z-axis is mediolateral (ML). In this paper, the term 'ML axis' is preferred over 'transverse axis' to minimize confusion with references to the transverse plane. XY planes are sagittal planes, XZ planes are frontal (coronal) planes, and YZ planes are transverse planes. Shear forces act within named planes: sagittal shear forces act within sagittal planes, frontal shear forces act within frontal (coronal) planes, and transverse shear forces act within transverse planes. Following [Hibbeler \(2000\)](#), positive shear forces rotate bodies clockwise looking from the right side, top, or front (i.e., toward the origin of the coordinate system). Shear forces are associated with sagittal, frontal, and transverse shear strains and deformations in those planes. Positive shear strain is a decrease in the angle of the corner of a square element at the intersection of the coordinate system axes. Moments or torques are described as acting about anatomical axes, with positive and negative moments following the right-hand rule. Moments around the Y-axis or AP axis that tend to evert the base of the right mandible or invert the base of the left mandible are negative AP moments or torques. Positive moments around a vertical axis (X-axis) through the right mandible—laterally wishboning the balancing-side mandible—are positive SI moments or torques. Positive moments about an ML axis are positive ML moments or torques. Because of the shape of the mandible: AP moments (torques about AP axes) through the corpus and ramus are twisting moments; ML moments (torques about ML axes) through the corpus and ramus are sagittal bending moments; ML moments through the symphyseal region are ML twisting moments; and SI moments anywhere through the mandible are transverse bending moments. Positive sagittal bending is concave superiorly (the shape holds water; [Hibbeler, 2000](#)). Axial strains are positive (tensile) or negative (compressive) strains in planes parallel to the coordinate system axes. Although axial strains are not usually discussed in the literature, they provide useful insight into the strain and deformation regimes associated with calculated loading regimes.

A variety of theories of mandible mechanics has been proposed. In this paper, we focus on those that have been most influential on ideas about anthropoid primate mandible mechanics and on the kinds of bony measurements that functional morphologists use to study links between mandibular form and feeding behavior or diet.

1.1. The balancing-side corpus

According to current theories of mandible mechanics, the balancing-side corpus is subject to negative sagittal bending (concave inferiorly), negative sagittal shear (more posterior sections are forced superiorly relative to more anterior sections), lateral transverse bending (lateral 'wishboning'), and negative AP twisting (eversion of the basal border; [Hylander, 1979b, c, 1981, 1985](#)). For definitions of the coordinate system and terms such as negative bending and negative shear, see [Figure 1](#). Sagittal shear forces are hypothesized to be greatest in the ramus, between points of application of muscle and joint forces ([van Eijden, 2000](#)), or in the corpus ([Demes et al., 1984](#)); lateral transverse bending moments are hypothesized to increase from posterior to anterior ([van Eijden, 2000](#)), and AP twisting moments are expected to be constant along the corpus ([Demes et al., 1984; Hylander, 1979c](#)). A human-like deformation pattern would be "helically upward and towards the working-side" ([van Eijden, 2000: 131](#)), with sagittal deformation and negative twisting—eversion of the basal border ([Korioth et al., 1992](#)).

1.2. The working-side corpus

The working-side corpus below the postcanine teeth is hypothesized to be subject to positive sagittal bending, positive sagittal shear, lateral transverse bending, and AP twisting that varies with the bite point ([Hylander, 1979b, c, 1981, 1985](#)). In chewing or biting along the anterior postcanine teeth, as modeled here, the anterior corpus is subject to negative AP twisting (inversion of the basal border), and the ramus is subject to positive AP twisting (eversion of the basal border). Sagittal shear is hypothesized to be largest between the bite point and the muscle insertion points on the ramus ([Demes et al., 1984; Hylander, 1979c; van Eijden, 2000](#)); lateral transverse bending moments are hypothesized to increase from posterior to anterior ([van Eijden, 2000; Vinyard and Ravosa, 1998](#)) or to peak at the bite point ([Demes et al., 1984](#)); and AP twisting moments are argued to vary with the bite point, with relative magnitudes of muscle and bite force, and along the corpus ([Demes et al., 1984; Hylander, 1979c](#)). Human-like deformation of the working-side mandible has been described as a predominance of sagittal bending over twisting, with the twisting characterized by inversion of the basal border ([Korioth et al., 1992](#)).

1.3. The symphyseal region

The symphyseal region is hypothesized to be subject to positive frontal bending, negative frontal shear, lateral transverse bending, and negative ML twisting ([Hylander, 1984](#)). Positive frontal bending is thought to be the result of a combination of negative AP torsion of the balancing-side mandible and positive AP torsion of the working side—eversion of the basal mandible on both sides. Negative frontal shear is thought to be due to a combination of superior components of balancing-side muscle force and inferior components of bite force ([Beecher, 1977; Demes et al., 1984; Hylander, 1984; Korioth and Hannam, 1994; Korioth et al., 1992](#)). Lateral transverse bending late in the power stroke is hypothesized to be due to laterally (to the balancing side, to the right in our model) directed components of balancing-side deep masseter force pulling the balancing-side mandible laterally, while the bite force and residual (decreasing) force from the working-side superficial masseter pull the working-side mandible in the opposite direction ([Hylander, 1984; Hylander and Crompton, 1986; Hylander and Johnson, 1994, 1997; Hylander et al., 1987](#)). The question of the direction of ML twisting is as yet unresolved: some authors posit that positive twisting occurs because the moments associated with upward components of balancing-side muscle force are larger than moments associated with inferiorly directed joint reaction force ([Wolff, 1984; Wolpoff, 1980](#)). Others hypothesize negative ML twisting owing to large torques associated with the balancing-side joint reaction force ([Hylander, 1984](#)).

1.4. The ramus

The inaccessibility of the ramus for in vivo strain gauge recordings has resulted in its neglect in most recent work on primate mandible biomechanics. Older studies suggested that various external features of the ramus, including the endocondylar ridge, ectocondylar crest, endocoronoid crest, and external oblique line, function to strengthen the ramus against muscle forces being transmitted to the corpus ([Walkhoff, 1902; Weidenreich, 1936](#)). As noted previously, in chewing or biting along the anterior postcanine teeth, the ramus is hypothesized to be subject to positive AP twisting, and sagittal shear is hypothesized to be largest between the bite point and the muscle insertion points on the ramus ([Demes et al., 1984; Hylander, 1979c; van Eijden, 2000](#)).

2. Materials and methods

The finite element model used in this paper is that presented by Panagiotopoulou et al. (2017). We used the material properties, loading, and constraint conditions that resulted in the best validated model from that study. The geometry of the skull was captured by computed tomography on a Philips Brilliance Big Bore scanner at the University of Chicago. The scans were processed in Mimics Materialise software v. 17 (Materialise, Belgium) to segment out the mandible and extract 3D surface data sets of the cortical bone, trabecular bone tissue, teeth, periodontal ligament, and mandibular bone screws (used to measure jaw kinematics). The bone screws (2.7 mm × 10 mm Vitallium cortical bone screws [OFSQ13; 3I Implant Company, West Palm Beach, FL, USA]) were included in the model because they were present in the animal during the in vivo validation recordings reported in Panagiotopoulou et al. (2017). The 3D data sets of all materials were assembled to create a 3D nonmanifold file in Materialise 3-matic v. 10 (Materialise, Belgium) and converted into volumetric mesh files of solid continuum linear tetrahedral elements (C3D4) for finite element analysis. The whole assembly has 622,134 elements, and the maximum nominal element size is 0.7 mm.

Isotropic, homogeneous, and linear elastic material properties were assigned to the periodontal ligament ($E = 6.80 \times 10^{-4}$ GPa; $\nu = 0.49$), teeth ($E = 24.5$ GPa; $\nu = 0.3$), bone screws ($E = 105$ GPa; $\nu = 0.36$), and trabecular bone tissue ($E = 10$ GPa; $\nu = 0.3$; Panagiotopoulou et al., 2017). The cortical bone was modeled as heterogeneous and orthotropic using subject-specific measurements of bone properties with the ultrasound wave technique (Dechow et al., 2017). Tie constraints (frictionless constraints) were used to bind together all intersecting surfaces.

To simulate the bite force, we constrained all translations at nodes on the occlusal surface of the left P_3 (35 nodes), P_4 (32 nodes), and M_1 (78 nodes). One node on the top of the left (working side) mandibular condyle was fixed against displacement in all directions; one node at the top of the right condyle was fixed against AP and SI but not ML displacement (Panagiotopoulou et al., 2017).

To determine how mastication on foods of different material properties affects deformation and strain regimes in the mandible, we applied three different loading regimes, associated with chewing on foods of three different material property types—fresh grapes with skins, dried fruits, and nuts (Reed and Ross, 2010). Muscle force magnitudes were estimated using in vivo EMG data recorded during a single feeding session in which the animal was fed on softer food (grapes) with relatively low toughness ($R = 125 \text{ Jm}^{-2}$) and low stiffness ($E = 0.6$ MPa), dried fruits (prune, dry apricot/cranberry/pineapple, date, gummy bear) characterized by relatively high toughness ($590 \leq R \leq 1059 \text{ Jm}^{-2}$) and low stiffness ($0.5 \leq E \leq 6.0$ MPa), and nuts (shell-less almond, cashew, brazil nut, pecan, walnut), characterized by relatively low toughness ($105 \leq R \leq 166 \text{ Jm}^{-2}$) and high stiffness ($8 \leq E \leq 34$ MPa; Reed and Ross, 2010; Ross et al., 2009; Williams et al., 2005; Supplementary Online Material [SOM] Fig. S1). The highest EMG amplitude recorded from each muscle was assumed to correspond to recruitment of 100% of that muscle's physiological cross-sectional area (PCSA), and the EMG amplitudes were scaled linearly (Weijs, 1980; Weijs and Dantuma, 1975; Weijs and Van Ruijven, 1990).

Estimates of muscle PCSAs for our experimental subject were made following standard dissection methods described elsewhere (Anapol et al., 2008; Shahnoor, 2004; Taylor et al., 2009, 2015; Taylor and Vinyard, 2009, 2013) using the following equation:

$$\text{PCSA (cm}^2\text{)} = (\text{muscle mass [g]} \times \cos \theta) / (\text{fiber length [cm]} \times 1.0564 \text{ g/cm}^3)$$

where 1.0564 g/cm^3 is the specific density of muscle (Mendez and Keys, 1960), normalizing fiber length by sarcomere length following Felder et al. (2005). Instantaneous force estimates were calculated as follows: the mean normalized EMG amplitude at time of maximum strain magnitude in the lower lateral gage × estimated PCSA × specific tension of muscle (30 N/cm^2 ; Sinclair and Alexander, 1987). Muscle forces were applied at surface nodes representing the insertion of the jaw muscles—anterior and posterior temporalis, deep and superficial masseters, and medial pterygoids—estimated from dissection of the experimental subject (SOM Fig. S1). Muscle force orientations were calculated using vectors running from the centroids of the insertions on the mandible to the centroids of the origins on the cranium (SOM Fig. S2; Panagiotopoulou et al., 2017). Table 1 gives the X, Y, and Z components of the muscle force vectors estimated from electromyography recorded during chewing of the three food types, as well as the components of the reaction force vectors acting at the condyles and bite points.

Loading regimes were quantified using moments and shear forces. Following convention, twisting moments (torques) act about the long (AP, Y) axis of the mandible, and bending moments act about the orthogonal axes. Sagittal bending moments act about the transverse (ML, Z) axis, and transverse bending moments act about the vertical (SI, X) axis. Moments were calculated in Abaqus CAE Simulia v. 6.13 (Dassault Systèmes, Vélizy-Villacoublay, France) about coordinate axes through centroids of cross sections (Fig. 2). Shear forces pull adjacent parts of the mandible in opposite directions and are calculated in sagittal (XY), frontal (XZ), and transverse (YZ) planes (Fig. 3). Shear forces were calculated in Excel 2010 (Microsoft Corporation, Redmond, Washington, USA).

The FEM was solved using the Abaqus default implicit direct static solver and Newtonian default iterations. Solution time, using four processors and eight tokens, was approximately 10 min per model. Deformation regimes were examined using static images of deformed and undeformed models (SOM Fig. S3) as well as animations of 1–70× scaled deformations of the deformed model (SOM File S1). It is important to note that the animations in SOM Figure S1 are not dynamic representations of changing patterns of deformation through the power stroke: rather, they show linear increases in deformation magnified 70×. The distributions of axial (X, Y, Z), principal, and shear strains were examined using figures of the models, with colors representing strain magnitudes. To compare strain regimes associated with different food types, strain magnitudes were extracted from surface elements under different loading conditions; then, the difference values were calculated and plotted on the surface of the models using a color scale.

All in vivo primate work was conducted at the University of Chicago under Animal Care and Use Protocol 72154.

3. Results

3.1. Loading, deformation, and strain regimes during chewing

We first asked whether loading and deformation regimes in our macaque FEM match those hypothesized for the power stroke of mastication (Dechow and Hylander, 2000; Demes et al., 1984; Hylander, 1979b, c, 1984, 1985, 1988; Hylander et al., 1987; Koriath et al., 1992; van Eijden, 2000; Wolff, 1984). Hypotheses about loading and deformation regimes underlie decisions about measurements made by functional morphologists attempting to link

Table 1

Loading regime: forces and force components (N) acting on the model during simulation of the power stroke on three food types.

Muscle forces	Total	Grapes			Total	Dry fruits			Total	Nuts		
		x	y	z		x	y	z		x	y	z
Anterior temporalis												
Left	35.2	33.63	-9.90	3.50	18.3	17.46	-5.14	1.82	32.9	31.45	-9.26	3.27
Right	23.2	22.61	-5.32	0.71	18.2	17.72	-4.17	0.55	45.5	44.23	-10.41	1.38
Posterior temporalis												
Left	33.9	14.81	-16.83	4.16	10.3	6.72	-7.64	1.89	16.2	10.53	-11.97	2.96
Right	33.6	8.08	-9.29	-0.76	14.0	9.14	-10.51	-0.86	37.8	24.76	-28.47	-2.34
Superficial masseter												
Left	33.1	13.93	8.58	6.29	28.2	22.45	13.82	10.13	63.4	50.41	31.03	22.76
Right	32.7	41.14	14.47	-20.91	17.3	14.79	5.20	-7.53	32.4	27.62	9.70	-14.06
Deep masseter												
Left	17.9	5.09	-0.96	4.87	3.4	2.46	-0.47	2.35	4.9	3.54	-0.67	3.38
Right	19.7	6.49	-0.41	-5.62	10.3	7.78	-0.52	-6.77	25.2	19.04	-1.28	-16.57
Medial pterygoid												
Left	27.6	8.44	1.79	-3.49	24.4	22.17	4.69	-9.17	43.7	39.65	8.38	-16.41
Right	29.0	23.55	4.42	11.32	6.4	5.72	1.07	2.75	15.9	14.13	2.65	6.79
Reaction forces												
Left condyle		-26.77	10.24	-2.10		-31.14	3.34	-3.33		-56.61	1.45	-7.08
Right condyle		-75.95	-1.20	0.00		-42.35	3.95	0.00		-99.67	18.31	0.00
Left M ₁		-53.59	-2.98	22.38		-43.52	-6.32	14.90		-84.62	-13.92	30.85
Left P ₄		-9.67	2.77	1.06		-6.12	0.07	2.34		-12.81	-0.42	5.12
Left P ₃		-11.68	4.65	-21.46		-3.22	2.62	-9.12		-11.49	4.86	-20.17

mandibular morphology to feeding behavior and diet. This question was addressed using results from modeling of nut chewing during which moments, shear forces, and strain magnitudes were the highest in comparison with other food types. We then described the strain regimes in the corpus, ramus, and symphysis associated with these loading and deformation regimes. Loading regimes are given in Figure 3. Deformation and strain regimes for the balancing side are shown in Figure 4, for the working side in Figure 5, and for the symphyseal region in Figure 6. Axial, shear, and principal strains during nut chewing are shown in SOM Figures S4–S7. Deformation animations are shown in SOM File S1.

3.2. Balancing-side (right) corpus

Loading and deformation regime Consistent with our hypothesis, the balancing-side corpus is subject to negative sagittal bending, negative sagittal shear, lateral transverse bending, and negative AP twisting. The largest torques acting on the balancing-side mandible are positive ML–negative sagittal bending—moments associated with inferiorly directed components of bite force transmitted across the symphysis (Fig. 2). These moments increase posteriorly until opposed by the negative torques exerted by superior components of balancing-side jaw elevator muscles (Fig. 2, frontal section no. 13). Negative sagittal bending moments are accompanied by negative sagittal shear forces (Fig. 3C), which are due to inferiorly directed components of force crossing the symphysis from the biting side, superiorly directed components of balancing-side jaw elevator muscles acting on the ramus, and inferiorly directed components of joint reaction force (Fig. 4B, F). These negative sagittal shear forces, larger in the posterior ramus than in the corpus (e.g., van Eijden, 2000), deform the balancing-side angle, ramus, and coronoid process upward relative to the corpus (Fig. 4A, B).

The balancing-side mandible is also subjected to negative vertical torques (Fig. 2)—and associated positive transverse shearing forces (Fig. 3D)—which produce lateral transverse bending deformation of the balancing-side (right) angle, condyle, ramus, and most of the corpus (Fig. 4A, B; SOM Figs. S5 and S6). The balancing-side mandible is also subject to low-magnitude negative AP torques (Fig. 2), causing eversion of the basal border (Hylander, 1979c;

Fig. 4A; SOM Fig. S6). However, rather than being constant along the corpus (Demes et al., 1984; Hylander, 1979c), these AP torques increase in the anterior corpus, peaking at the level of P₄.

The overall deformation of our macaque FEM (SOM Fig. S6) resembles that of the model of a human mandible by Koriath et al. (1992: Fig. 3; see also Koriath and Hannam, 1994): in deformation, the mandible appears to rotate around the bite point, with the balancing-side mandible basal border everting and the alveolar process inverting.

Strain regime Negative sagittal bending of the balancing-side corpus is associated with high-magnitude tensile AP and ϵ_1 strains on the superior and medial surfaces of planum alveolare, the extramolar sulcus, and the alveolar prominence (Fig. 4H, I). Sagittal shear forces are associated with negative sagittal shear strain in the buccal surface of the corpus, especially the external oblique line (Fig. 4F, G). Lateral transverse bending is associated with tensile AP strain and high-magnitude ϵ_1 on most of the lingual surface (Fig. 4I), compressive AP strain on the buccal surface of the mandible (Fig. 4J), and positive transverse shear strains on the superior surface of planum alveolare, the extramolar sulcus, and the alveolar prominence (SOM Fig. S5N, Q). AP compression is not uniformly distributed on the buccal surface; superposition of lateral transverse bending on negative sagittal bending results in high values of AP compression (Fig. 4K) and ϵ_2 on the buccal aspect of the basal corpus (Fig. 4L). Negative AP torsion of the balancing-side mandible is associated with positive transverse shear strain on the superior surface of the planum alveolare, the extramolar sulcus, and the alveolar prominence (Fig. 4C) combined with negative transverse shear strains on the basal surface (Fig. 4D).

3.3. Working-side (left) corpus

Loading and deformation regime As hypothesized, the working-side mandible below the bite point on P₄ and M₁ is subjected to negative ML (positive sagittal bending) moments, positive vertical (lateral transverse bending) moments, and negative AP moments. The effects of these torques on the anterior working-side corpus—under the bite point—are positive sagittal bending, lateral transverse bending, and negative AP torsion, inverting the basal border below the bite point (Fig. 5A, B; SOM Fig. S6).

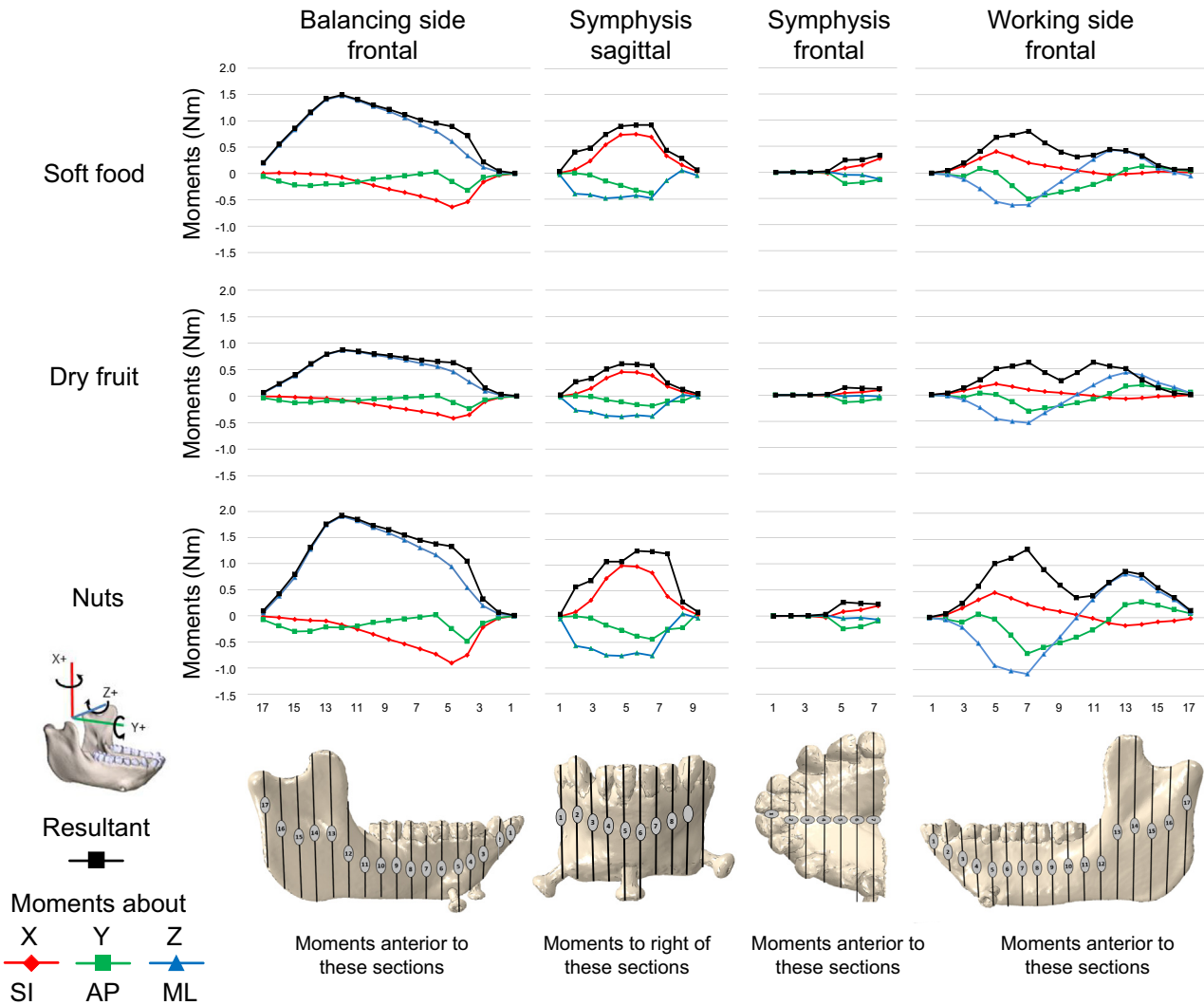


Figure 2. Moments (in N m; force [N] \times distance [m]) acting about axes parallel to the coordinate system on the working side, on the balancing side, and through the symphyseal region. Numbers on the ordinate correspond to section planes illustrated in the figures at bottom. Moments about X axes are SI moments (i.e., moments about SI axes) or transverse bending moments (i.e., moments that bend in transverse planes); moments about Y axes are AP or twisting moments; moments about Z are ML or sagittal bending moments. Balancing-side frontal and working-side frontal: these moments are calculated as the sums of all the moments acting on the bone anterior to frontal planes through the illustrated sections. This includes those moments acting on the contralateral hemimandible, whether behind or in front of the section plane. Symphysis frontal: moments about frontal planes through the symphyseal region summed anterior to the illustrated sections. Symphysis sagittal: moments about sagittal planes through the symphyseal region summed to the right of the illustrated sections. For example, moments acting on the midsagittal plane are the sum of all balancing-side moments. Abbreviations: SI = superoinferior; AP = anteroposterior; ML = mediolateral.

Torques are not constant along the corpus: in the posterior corpus, transverse, vertical, and AP torques decrease to zero at or immediately behind M_3 before reversing in the ramus (see below; Fig. 2). Despite this reversal, the basal border of the entire working-side mandible is inverted in deformation (SOM Fig. S6). As hypothesized, sagittal shear forces are highest between the bite points on the tooth row and the ramus (Demes et al., 1984; Hylander, 1979c; van Eijden, 2000). However, contrary to our hypothesis, negative (as opposed to positive) sagittal shear is high along the length of the mandible (Figs. 3 and 5F), deforming the retromolar fossa upward (Fig. 5B; SOM Fig. S6).

Strain regime Positive sagittal bending deformation about the bite point is associated with compressive AP strain along the buccal and lingual sides of the alveolar process and in the upper surface of planum alveolare lingual to the premolars, canines, and incisors (Fig. 5H, J, K). It is also associated with relatively high-magnitude tensile AP and ϵ_1 strains in the base of the corpus below the bite point (Fig. 5K–M). On the buccal surface of the

working-side corpus, AP variation in shear forces is associated with variation in sagittal shear strains: these shear strains are positive in front of the bite point, negative immediately behind it, and then positive further posteriorly in the ramus (Fig. 5F, G). Negative AP torsion of the anterior working-side corpus is associated with positive transverse shear strain on the superior surface of the corpus and negative transverse shear strain in the base of the mandible (Fig. 5C, D). ϵ_1 is oriented upward and backward on the buccal side of the corpus, below m_3 , and upward and forward on the lingual side (Panagiotopoulou et al., 2017; Fig. 10).

3.4. Symphyseal region

Loading and deformation regime A hypothesis of positive frontal bending is corroborated by the moments acting on the symphysis (Fig. 2) and by the deformation regime (Fig. 6A, E; SOM Fig. S6).

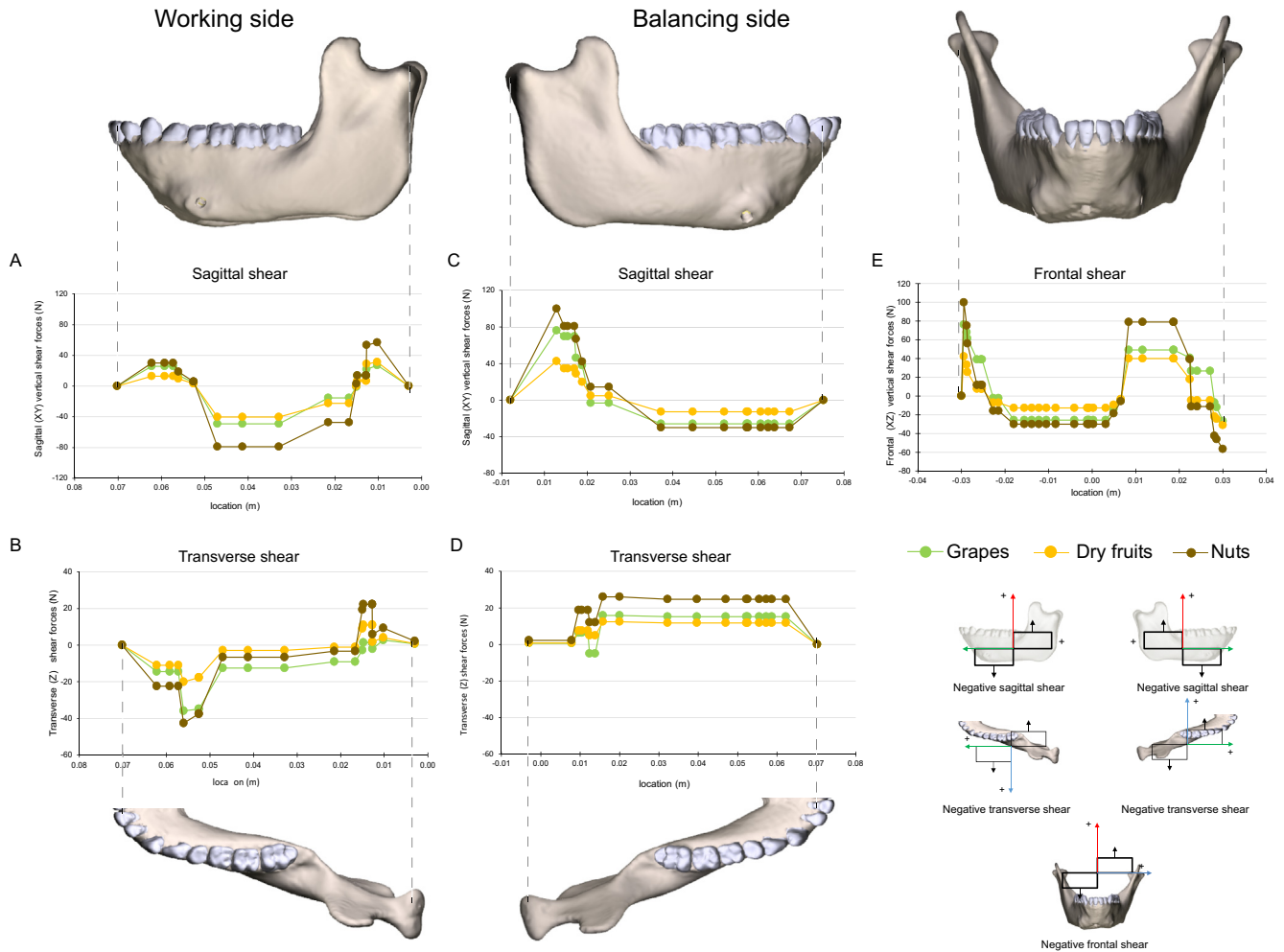


Figure 3. Shear forces in newton (N) acting within specified planes. Sagittal and transverse shear forces are sums of all forces anterior to each coronal plane. Frontal shear forces are sums of all forces to one side of the specified plane. Images of the mandible model are aligned to planes for which forces were calculated. A) Working-side vertical, sagittal plane shear forces. B) Working-side transverse plane shear forces. C) Balancing-side vertical, sagittal plane shear forces. D) Balancing-side transverse plane shear forces. E) Frontal shear forces plotted against mandible width. The key in bottom right illustrates polarity of shear (cf. Fig. 1).

However, contrary to accepted models (Beecher, 1977; Hylander, 1984), this positive frontal bending is associated with negative AP moments in both working- and balancing-side mandibles (Fig. 2; SOM Fig. S6). These moments, maximum in a near-frontal plane through the balancing-side P₄ and working-side M₁, twist the symphysis and balancing-side corpus about the bite point, resulting in positive frontal bending deformation, with a center of flexure at the bite point (clockwise in anterior view; Figs. 4C, D and 5C, D; SOM Fig. S6). A hypothesis of negative frontal shear deformation of the symphysis is corroborated by the loading (Fig. 3) and deformation regimes (Fig. 6E; SOM Fig. S6). However, if negative frontal shear loading and deformation regimes were predominant in the symphyseal region, both labial and lingual surfaces of the symphysis would experience negative frontal shear strain. In contrast, negative frontal shear strain in the labial surface (Fig. 6H) is accompanied by positive frontal shear strain in the lingual surface (Fig. 6D; see below). Similarly, the symphyseal region is also characterized by transverse shear of opposite signs on superior and inferior surfaces (Fig. 7J; SOM Fig. S5Q, R). Shear strains of opposite sign on opposing surfaces are indicative of torsion, and the loading and deformation regimes confirm a hypothesis of negative ML twisting (Hylander, 1984), not positive ML twisting (Demes et al., 1984; Wolff, 1984; Wolpoff, 1980; Fig. 6I–K). These negative ML twisting moments

are primarily because of large inferiorly directed components of balancing-side joint reaction force (–100 N) acting about a long moment arm (0.064 m), yielding a negative ML torque of 6.4 Nm (Fig. 6I; Table 2). This is countered by positive ML torques associated with anteriorly directed components of balancing-side joint reaction force and superior components of balancing-side jaw elevator muscle force, but the net effect is a negative 0.7 Nm ML twisting moment through the symphysis (Fig. 6I–K). The deformation regime of the symphyseal region provides visual confirmation of the loading regime: the anterior region of the balancing-side mandible deforms upward relative to the jaw joint (Fig. 6E; SOM Fig. S6).

A hypothesis of lateral transverse bending (lateral ‘wishboning’) is corroborated by the negative vertical torques in the balancing-side symphyseal region (Fig. 2), negative transverse shear forces on the working-side symphysis, and positive transverse shear forces on the balancing-side symphysis (Fig. 3). As a result, the balancing-side condyle, angle, and corpus are deformed laterally relative to the working side (Fig. 6A, E).

Strain regime Lateral transverse bending of the symphyseal region is associated with high values of ML directed tensile strain in the lingual symphysis (Fig. 6B, C) and ML oriented compressive strain in the labial symphysis (Fig. 6F, G; Hylander, 1984). As discussed previously, negative ML twisting of the symphysis is associated

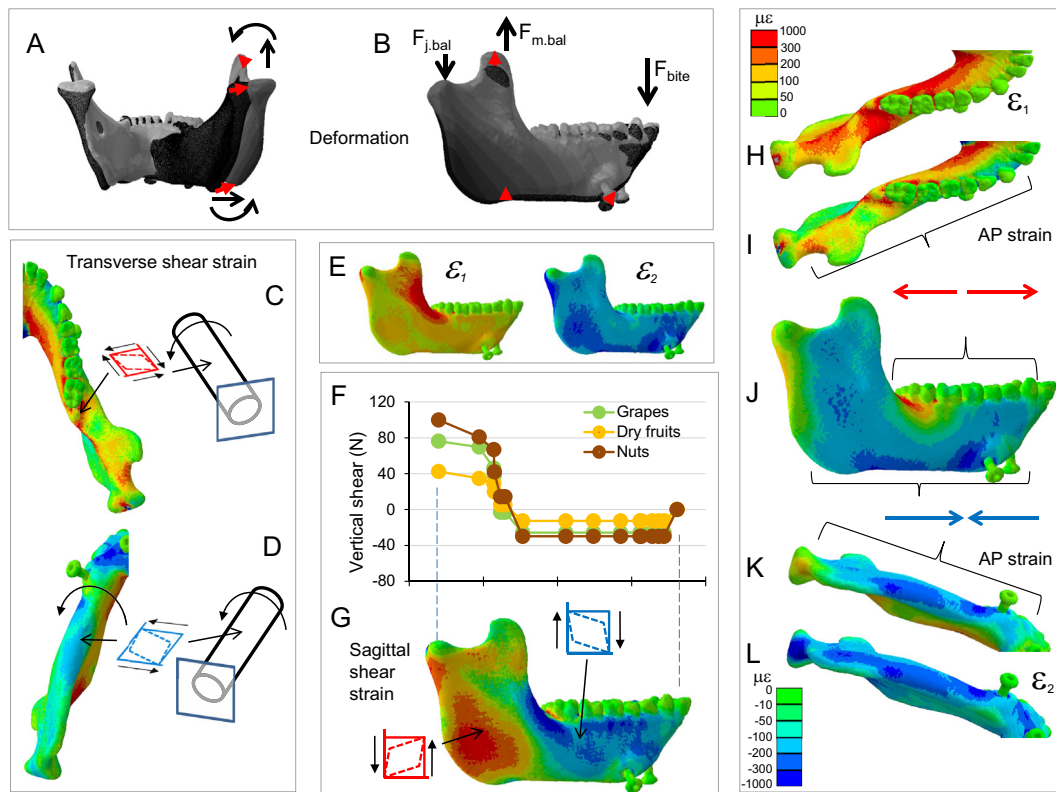


Figure 4. Deformation and strain regimes in the balancing-side corpus and ramus during simulation of nut chewing. Strain scales in H and L apply to principal, axial, and shear strains. A, B) Model deformation, in posterior (A) and lateral (B) views. The left side is the working (biting) side; the right side is the balancing side; the left P_3 , P_4 , and $M1_1$ are constrained against all displacements; the deformed model is transparent; the undeformed model is solid; the deformation scale factor is 70. Red arrows connect homologous points between undeformed and deformed models; curved black arrows indicate negative AP twisting of the balancing-side mandible; straight black arrows indicate lateral transverse bending. $F_{j.bal}$ = vertical component of balancing-side joint reaction force; $F_{m.bal}$ = vertical component of balancing-side muscle force; F_{bite} = vertical component of bite force. C, D) Transverse shear strain and AP twisting: positive transverse shear strain along the top of the corpus and endocondylar ridge (C) and negative transverse shear strain along the bottom of the balancing-side mandible (D) are associated with negative AP twisting. E) Maximum (ϵ_1) and minimum (ϵ_2) principal strain regimes in the lateral surface of balancing-side mandible. F) Sagittal shear forces acting along the balancing-side mandible. G) Sagittal shear strain on the lateral surface of the balancing-side mandible. H–L) Anteroposterior (AP) strains (I–K) and principal strains (H, L) associated with negative sagittal bending of the balancing-side mandible. Maximum principal strain (ϵ_1) on the top of the balancing-side mandible (in H) is primarily due to AP tensile strain (in I). Minimum principal strains (ϵ_2) in the base of the mandible (in L) are primarily due to AP compressive strain (in K). The predominance of AP compressive strain in the lateral surface of the balancing-side mandible (in J) is due to lateral transverse bending of the mandible. The high values of AP compression (J, K) and of ϵ_2 along the lateral edge of the base of the mandible are due to superposition of lateral transverse bending and negative sagittal bending. Abbreviation: AP = anteroposterior. (For interpretation of the references to color in this figure legend, the reader is referred to the Web version of this article.)

with negative frontal shear strain on the labial surface and positive frontal shear strain on the lingual surface (Fig. 6D, H, K), along with positive ML shear strain on the superior surface and negative ML shear strain on the inferior surface (SOM Fig. S5Q, R).

The strain regime does not support the hypothesis that the symphysis is bent in frontal planes owing to positive AP twisting of the working-side mandible and negative AP twisting of the balancing side (Demes et al., 1984; Wolff, 1984). This loading regime would result in ML tensile strain in the lower half of the labial and lingual symphysis and ML compressive strain in the upper half of the symphysis. In fact, the entire midline lingual symphysis is in ML tension, and the lower labial symphysis is in ML compression.

3.5. The ramus

Loading and deformation regime The balancing-side ramus experiences large positive ML—negative sagittal bending—moments, which peak in frontal sections through the anterior ramus, external oblique line, and mandibular prominence, combined with low-magnitude negative AP moments and large positive sagittal shear forces (Figs. 2 and 3; SOM Fig. S6). The working-side ramus is subject to positive ML—negative sagittal bending—moments, the reverse of the negative bending regime

acting around the bite point. The working-side ramus is also subject to small positive AP twisting moments as well as positive transverse and sagittal shear forces (Figs. 2 and 3).

Strain regime Negative sagittal bending of the balancing-side ramus is associated with high-magnitude tensile AP and ϵ_1 strains on the superior surfaces of the extramolar sulcus, the anterior border of the ramus, the external oblique line, torus triangularis, and the endocondylar ridge (Fig. 4E, H, I). High-magnitude compressive AP and ϵ_2 strains are seen in the basal border of the ramus (Fig. 4J–L). Increasingly positive sagittal shear forces in more posterior sections are associated with a transition from high negative sagittal shear strains in the external oblique line to positive sagittal shear strains in the angle and posterior condylar neck (Fig. 4F, G). Lateral transverse bending and negative AP torsion of the balancing-side ramus result in positive transverse shear strains in the endocondylar ridge and the mandibular notch (Fig. 4C). The medial surface of the working-side ramus experiences mostly low-strain magnitudes, with the exception of positive sagittal shear strains along the endocondylar ridge and the back edge of the ramus (Fig. 5G; SOM Fig. S5B).

On the working side, negative sagittal bending is also associated with high-magnitude tensile AP and ϵ_1 strains on the superior surfaces of the extramolar sulcus, the anterior border of the ramus,

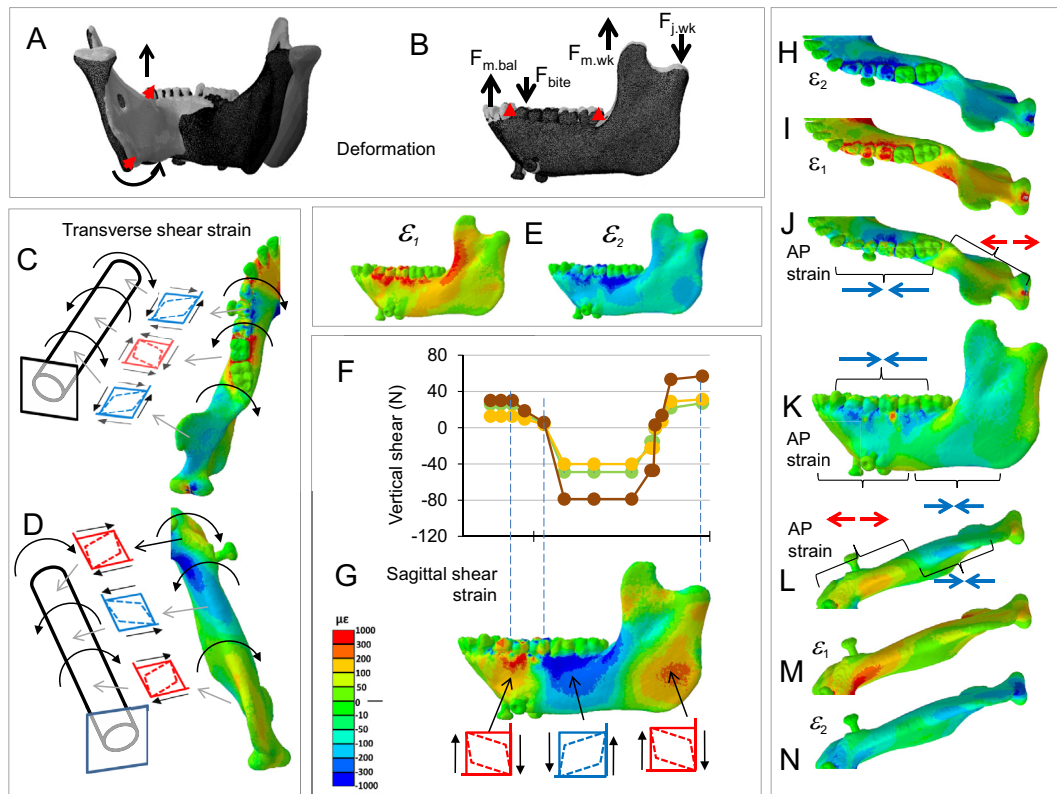


Figure 5. Deformation and strain regimes in the working-side corpus and ramus. Strain scale in G applies to principal, axial, and shear strains. A, B) Deformation regime: the left side is the working (biting) side; the right side is the balancing side; the left P_3 , P_4 , and M_1 are constrained against all displacements; the deformed model is transparent; the undeformed model is solid; the deformation scale factor is 70. Red arrows connect homologous points between undeformed and deformed models; curved black arrows indicate negative torsion of the working-side mandible. Thick black arrows indicate vertical force components: $F_{m.bal}$ = balancing-side muscle force transmitted across the symphysis; F_{bite} = bite force; $F_{m.wk}$ = working-side muscle force; $F_{j.wk}$ = working-side joint reaction force. C, D) Transverse shear strain and anteroposterior (AP) twisting: alternating positive and negative transverse shear strain along the top (C) and bottom of the working-side corpus (D) are associated with alternating patterns of AP twisting. E) Maximum (ϵ_1) and minimum (ϵ_2) principal strain regimes in the lateral surface of the working-side mandible. F) Shear forces acting along the working-side mandible. G) Sagittal shear strain on the lateral surface of the balancing-side mandible. Sagittal shear strains are positive between the bite force and $F_{m.bal}$, negative between F_{bite} and $F_{m.wk}$, and positive between $F_{m.wk}$ and $F_{j.wk}$. H–N) AP strains (J–L) and principal strains (H, I, M, N) associated with sagittal bending of the working-side mandible. Minimum principal strain (ϵ_2) on the top of the working-side mandible (in H) is primarily due to AP compressive strain (in J). Maximum principal strains (ϵ_1) in the base of the mandible (in M) are primarily due to AP tensile strain (in L). (For interpretation of the references to color in this figure legend, the reader is referred to the Web version of this article.)

torus triangularis, and the endocondylar ridge (Fig. 5E, I, J), combined with high-magnitude compressive AP and ϵ_2 strains on the basal border (Fig. 5J, L, N). Sagittal shear strains in the lateral surface transition from high negative strains in the oblique line to positive strains in the angle and posterior condylar neck (Fig. 4F, G). Positive AP—twisting—moments in the working-side ramus are associated with negative transverse shear strains in the extramolar sulcus, torus triangularis, endocondylar ridge, and mandibular notch (Fig. 5C) and with positive transverse shear strains on the basal border and angle (Fig. 5D).

In both working- and balancing-side rami, SI tensile strains are high along the anterior edge of the ramus and SI compressive strains are high along the posterior edge of the ramus (SOM Fig. S4A, B).

3.6. Effects of variation in food type: balancing-side (right) mandible

Loading and deformation regime Hypothesized effects of food material properties on mandibular loading and deformation regimes underlie attempts to link mandibular morphology to diet and feeding behavior. Loading regimes—moments and shear forces—associated with chewing on grapes, dried fruits, and nuts are shown in Figures 2 and 3; differences in the loading regime between nut and dried fruit chewing and between nut and grape chewing are shown in Figures 7 and 8. On the balancing side,

loading regimes during nut chewing are similar to those during dried fruit and grape chewing (Figs. 2 and 3), but nut chewing is associated with larger positive ML (sagittal bending) and larger negative vertical (lateral transverse bending) moments under the postcanine tooth row (Fig. 7), and larger vertical and transverse shear forces (Fig. 8). The largest differences in AP twisting moments are found under P_3 ; these are the smallest food-related effects on the balancing side.

Strain regime Figure 9 compares the magnitudes of the principal and shear strains across the surface of the model, which is calculated as follows: nut strains – fruit strains. As expected with higher sagittal bending moments, principal and shear strain magnitudes are higher during simulated nut chewing than during dried fruit chewing. The greatest differences in ϵ_1 between nuts and dried fruit are seen in the lingual symphysis (see below) and balancing-side mandible. ϵ_1 magnitudes are higher during nut chewing than during dried fruit chewing in (i) the inferior transverse torus, (ii) an oblique line extending from the superior transverse torus along the balancing-side medial prominence toward the M_3 (Fig. 9A, C), (iii) the balancing retromolar trigon and extramolar sulcus (Fig. 9B), and (iv) the endocondylar ridge (Fig. 9C). Differences in ϵ_2 strain magnitude are concentrated in the alveolar bone around the roots of the biting teeth (Fig. 9E–H) and in the posterior edge of the balancing-side ramus, below the condyle (Fig. 9G).

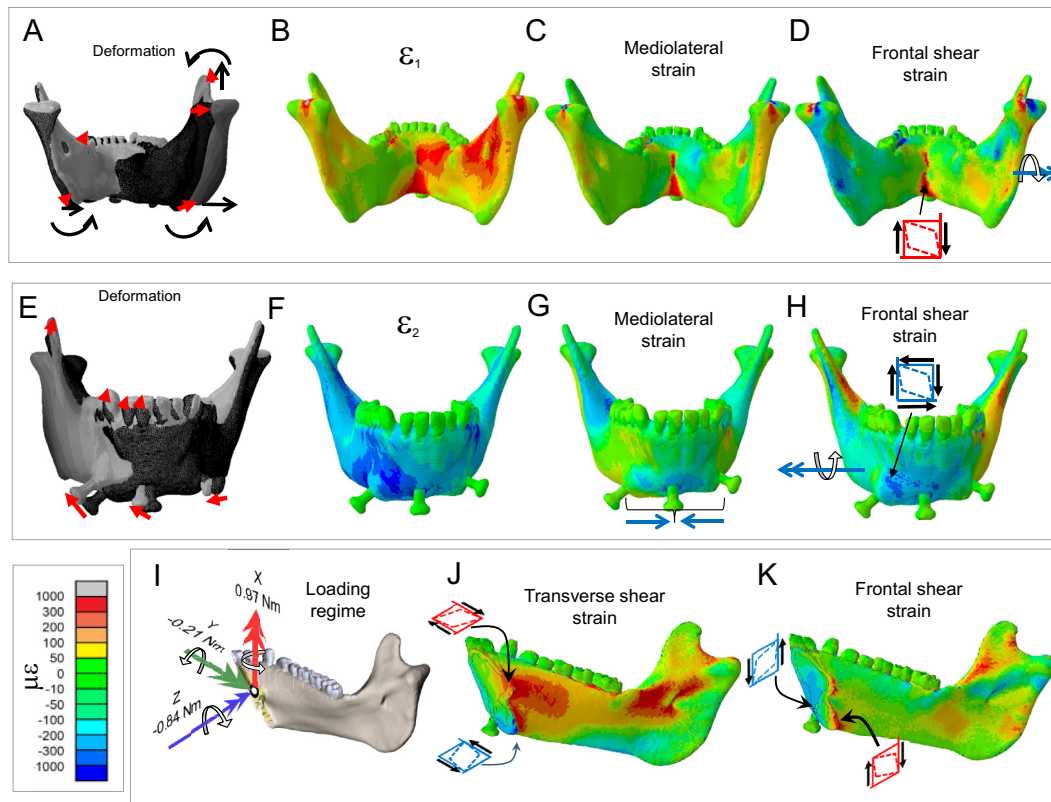


Figure 6. Deformation and strain regimes in the symphyseal region. The scale in bottom left applies to axial and shear strains. A, E) Deformation regime. Curved arrows indicate negative torsion of both working and balancing-side corpora and rami. Straight arrows indicate lateral transverse bending of the mandible. This deformation regime includes lateral transverse bending of the balancing-side corpus and ramus, such that the balancing-side (right) condyle displaces laterally, and medial bending of the working-side corpus by transversely (to the right) directed forces transmitted by the symphysis. A–D) Posterior view. E–H) Anterior view. I–K) Left posterior oblique view. B, F) Maximum (ϵ_1) and minimum (ϵ_2) principal strain regimes. C) Mediolateral tensile strains are high in the lingual symphysis in association with lateral transverse bending. G) Mediolateral compressive strains on the inferior labial symphysis are associated with lateral transverse bending. D, H) Frontal (coronal) plane shear strains are opposite in sign on lingual (D) and labial (H) surfaces of the symphysis in association with negative transverse twisting. I–K) Symphyseal loading and strain regime. I) Moments based on the balancing-side (right) free body, representing the moments acting on the working side of the symphysis during nut chewing (Fig. 2). The symphysis is subjected to negative transverse twisting, positive vertical twisting (lateral transverse bending), and negative AP twisting. The transverse (J) and frontal (K) shear strain regimes are reversed on opposite faces of the symphysis owing to negative transverse twisting.

There are large differences in magnitudes of balancing-side shear strains between nut and dried fruit chewing (Fig. 9I–T). The largest differences are in sagittal shear strains: during nut chewing, sagittal shear strains are larger in the front of the condylar neck, on the upper surface of the endocondylar ridge, on the lingual face of the balancing-side coronoid process, in the extramolar sulcus, and across most of the buccal side of the balancing-side corpus and symphysis (Fig. 9I–L). During nut chewing, the balancing-side mandible also experiences larger positive transverse (ϵ_{yz}) shear strains in the superior transverse torus of the symphyseal region, the medial and alveolar prominences, retromolar trigon, extramolar sulcus, torus triangularis, and endocondylar ridge (Fig. 9Q). These differences are associated with, and reflect, greater bending and torsion of the balancing-side mandible and larger vertical and transverse shear forces during nut chewing.

3.7. Effects of variation in food types: working-side (left) mandible

Loading and deformation regime On the working side, compared with grape and dried fruit chewing, nut chewing is associated with (Figs. 7 and 8) larger positive ML (negative sagittal bending) moments acting on the working-side ramus; larger negative ML (positive sagittal bending) moments immediately behind the bite point; larger positive vertical (transverse bending) moments on

the symphysis; larger negative AP twisting moments around the bite point; and larger negative transverse shear forces especially in the anterior corpus.

Strain regime Differences in the strain regime between nut and dried fruit chewing are less pronounced on the working side than on the balancing side. Higher magnitudes of ϵ_2 (Fig. 9E–H) and sagittal shear strain are evident in the lateral alveolar process around the working-side postcanine tooth roots (Fig. 9I–L). In association with increased sagittal shear forces, nut chewing is also associated with higher magnitude negative sagittal shear strains in the buccal surface of the working-side corpus below the molars, the working-side lateral prominence, and the external oblique line (Fig. 9I–L). The other principal and shear strain components in the working-side mandible are minimally impacted by variation in food types (Fig. 9).

3.8. Effects of variation in food types: symphyseal region

Loading regime Moments about frontal planes through the symphyseal region differ with food types (Figs. 2 and 7). During soft food (grapes) and nut chewing, the posterior symphyseal region is subjected to greater vertical moments (wishboning) and greater torques than during dried fruit chewing. However, the magnitudes of torques acting in frontal planes through the symphysis are low. The largest differences are in moments

Food effects on loading regime: Moments

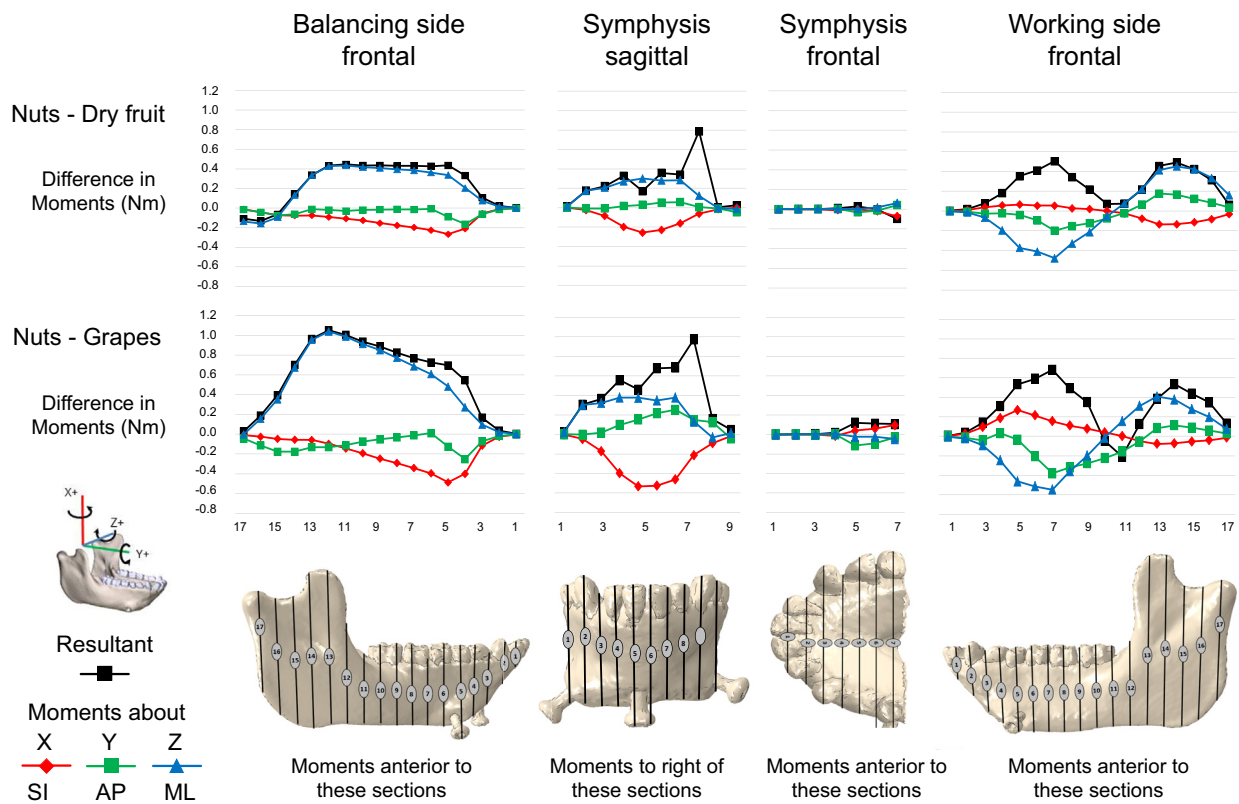


Figure 7. Food effects on moments. Plots of differences in moments calculated as follows: (moment during nut chewing) – (moment during grape or dried fruit chewing). All moments were of similar sign, so negative differences indicate nut chewing elicited larger negative moments, and positive differences indicate nut chewing elicited larger positive moments. Abbreviations: SI = superoinferior; AP = anteroposterior; ML = mediolateral.

Table 2
Moments (N m) acting anterior a section through working-side M₁.^a

Muscle	Fx*dz	Fz*dx
Left anterior temporalis	0	0
Right anterior temporalis	-1.59	0.03
Left posterior temporalis	0	0
Right posterior temporalis	-0.91	-0.07
Left superficial masseter	0	0
Right superficial masseter	-0.90	-0.022
Left deep masseter	0	0
Right deep masseter	-0.69	-0.30
Left medial pterygoid	0	0
Right medial pterygoid	-0.41	0.01
Left condyle	0	0
Right condyle	3.62	0 (unconstrained)
Left M ₁	-0.44	0.45
Left P ₄	-0.06	0.07
Left P ₃	-0.05	-0.31
Summed torques	Total Fx*dz = -1.44 Nm	Total Fz*dx = -0.13 Nm
Total torque	My = (Fx*dz) - (Fz*dx) = -1.31 Nm	

Abbreviations: Fx = forces in X direction (vertical, positive is up); Fz = forces acting in Z direction (mediolateral, positive is to animal left); dX = vertical distance between section centroid and muscle attachment or reaction force centroid; dZ = mediolateral distance between section centroid and muscle attachment or reaction force centroid; My = moments about Y-axis through M₁ centroid.

^a Entries are equal to 0 when they are moments acting on the mandible behind the section of interest (working-side M₁). Fz is 0 at the balancing-side condyle because the condyle is unconstrained in Z, so Fz*dz is 0.

calculated about sagittal sections. Relative to the other foods, nut chewing is associated with larger negative vertical moments, especially in the midline, and larger AP twisting moments and ML (sagittal bending) moments.

Strain regime There are large differences between nut and dried fruit chewing in strain magnitudes in the lingual symphysis. In both transverse tori, greater lateral transverse bending moments during nut chewing are associated with relatively higher magnitudes of ϵ_1 (Fig. 9C), and larger ML moments are associated with slight increases in negative sagittal (Fig. 9K) and positive frontal shear strains (Fig. 9O). In the inferior transverse torus, negative transverse shear strain is also greater during nut chewing (Fig. 9S). On the labial surface of the symphysis, ϵ_2 is larger inferiorly during nut chewing (Fig. 9H), and all of the shear strain components increase in magnitude. Sagittal shear strains become more negative on the balancing side and more positive on the working side of the labial surface (Fig. 9L); coronal shear strains become more negative, especially on the inferior half of the balancing side (Fig. 9P), and transverse shear strains become more negative on the balancing side (Fig. 9T). These increases in shear strains reflect increased—more negative—ML torques associated with nut chewing.

3.9. Maximum food type differences

The largest food-related differences in strain magnitude are mapped onto the mandible in Figure 10. Notable differences in magnitudes of principal strains and in sagittal and frontal shear strains are restricted to localized areas. For example, large

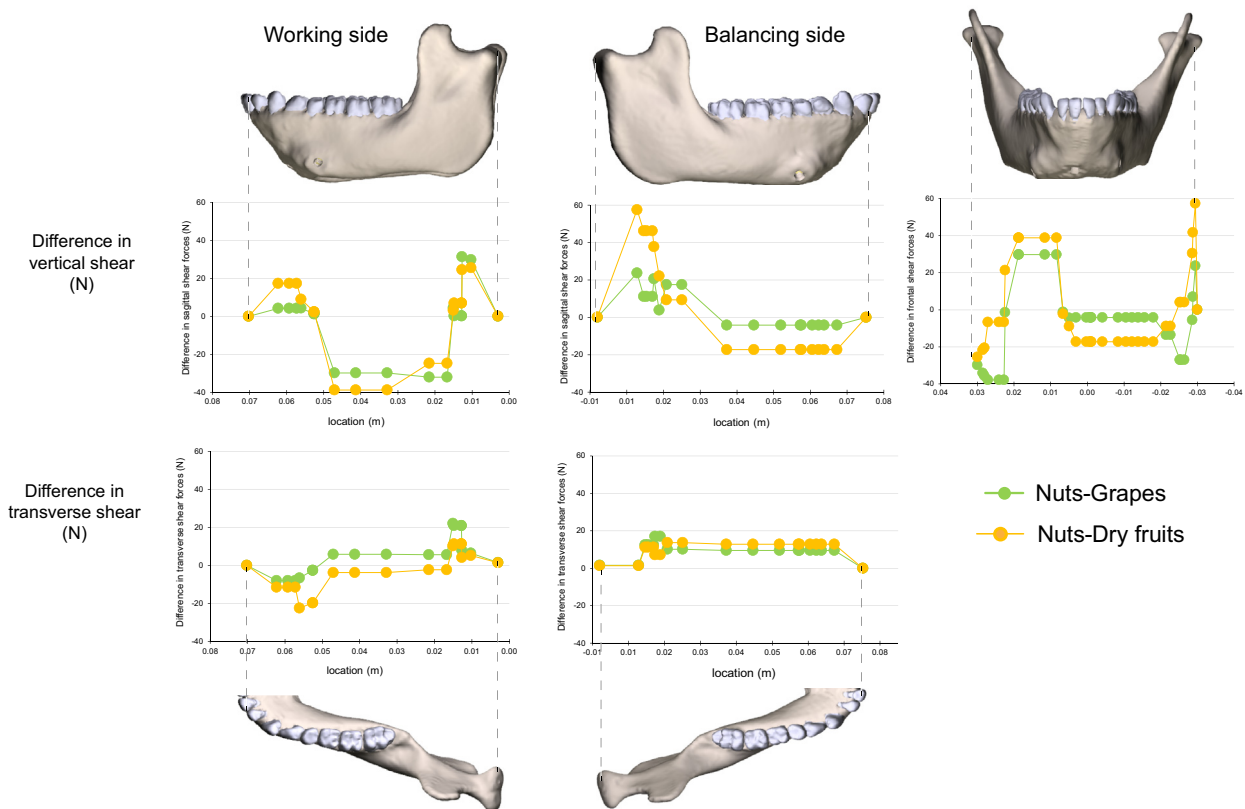


Figure 8. Food effects on shear forces. Plots of differences in shear forces calculated as follows: (shear during nut chewing) – (shear during grape or dried fruit chewing). All shear forces were of similar sign, so negative differences indicate nut chewing elicited larger negative shear, and positive differences indicate nut chewing elicited larger positive shear.

differences in ε_2 magnitude are restricted to the posterior condylar neck and ramus on the balancing side (Fig. 10G). Large differences in sagittal shear strain magnitudes are restricted to the buccal alveolar process on the working side and to recessus mandibulae and the lingual condylar neck on the balancing side (Fig. 10I). Large differences in frontal shear strain magnitudes are found in the inferior transverse torus (Fig. 10O, P). More significant are the large differences in ε_1 and transverse shear strains on the balancing side, extending from both the superior and inferior transverse tori along the anterior medial prominence, through the extramolar sulcus, and along the endocondylar ridge (Fig. 10A–D, Q–T). Maximum differences in the orientation of the maximum principal strains are shown in Figure 11. Food type effects on strain orientation are concentrated in the area of the working-side bone screw callus, the anterior condylar neck, and in a strip along the lingual surface of the working-side corpus below the mylohyoid line.

4. Discussion

This is the most detailed analysis of in vivo loading, deformation, and strain regimes in a mammalian mandible published to date, but some limitations should be borne in mind. Our focus is on hypotheses specific to *Macaca* because macaque in vivo strain data have provided the model for so much of the comparative work on mandibular form and diet in primates. However, similarities in mandible shape (Daegling, 2002) and muscle firing patterns across anthropoids (Hylander, 1981, 1984, 1988; Hylander and Crompton, 1986; Hylander and Johnson, 1994, 1997; Hylander et al., 1987, 1998, 2000, 2002, 2004, 2005, 2011) make our results relevant especially to cercopithecids, but also to other anthropoids, including humans and other hominids. The present study also only documents loading, deformation, and strain regimes at one point in time during the gape cycle: when, during our

in vivo recordings, peak shear strain magnitudes were recorded from the lower half of the lateral prominence on the corpus. Mandibular loading and strain regimes vary throughout the gape cycle (Hylander et al., 1987; Ross and Iriarte-Diaz, 2019). Thus, ongoing studies are aimed at a fuller understanding of mandible biomechanics throughout the power stroke. It should also be noted that the modeled mandible exhibited bone calluses superior to the two lateral bone screws, and these may have affected the local strain environment. Consequently, our discussion of strain regimes emphasizes strains in other parts of the mandible. Finally, we also note that transverse bite forces at the P₃ act toward the right, the reverse of the direction at the P₄ and M₁. This occurs because fixing the tooth surface against displacement fixes it against forces either pushing or pulling against the tooth surface. This effectively reduces the laterally directed component of bite force and negative torques acting on the anterior working-side tooth row. Our emphasis on modeling the in vivo experimental context as accurately as possible caused us to retain the excess bone and the fixed P₃ in this version of our model, the latter because these constraining conditions yielded the strain values that most closely matched those previously recorded in vivo (Panagiotopoulou et al., 2017).

4.1. Loading regimes

Current theories of macaque mandibular function make assumptions about the loading regime (Hylander, 1979b, c, 1981, 1984, 1986; Hylander et al., 1987), and these assumptions underlie hypotheses about mandible design in extant and fossil hominids (Daegling, 1989, 2001, 2007a, b; Daegling et al., 2016; Daegling and Grine, 2006; Hylander, 1988; Ravosa, 1988, 2000; Taylor, 2002, 2006a, b). Most of these assumptions have not been tested because the necessary combination of EMG, PCSA, anatomical, and strain

Nut vs. dried fruit chewing

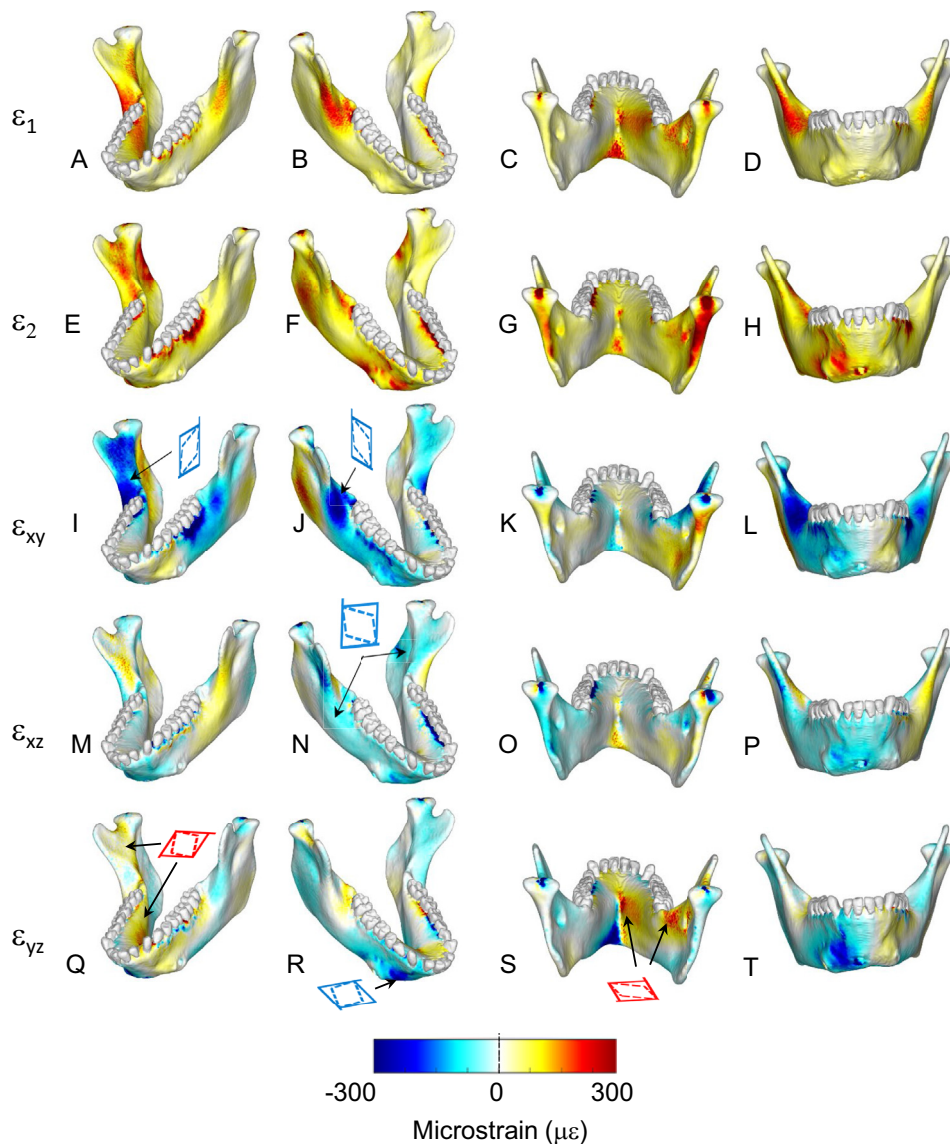


Figure 9. Comparisons of magnitudes of strain components from simulations of mastication of nuts and dried fruit. The scale applies to all figures (principal and shear strains). Figures map the distribution of differences in principal and shear strains recorded on the surfaces of the model during simulation of the power stroke of mastication on nuts and dried fruit. The top two rows (A–H) present principal strains; the bottom three rows (I–T) present shear strains. For principal strains, the comparisons are calculated as differences in absolute values (i.e., magnitudes) for ϵ_1 and ϵ_2 . For example, comparison of nut and dried fruit strain magnitudes reveals that along the endocondylar ridge, ϵ_1 magnitudes were ca. 300 $\mu\epsilon$ greater during nut chewing (A–D), and along the back edge of the ramus, ϵ_2 magnitudes were ca. 300 $\mu\epsilon$ greater during nut chewing (E–H). For shear strain comparisons, the differences are direct comparisons calculated as follows: (nut strain) – (fruit strain). The scale bar at the bottom indicates the difference in microstrain ($\mu\epsilon$) between the two simulations.

data has not been available until recently (Panagiotopoulou et al., 2017). In the present study, mandibular loading regimes were calculated using EMG data collected when in vivo strain magnitudes in the lower lateral prominence of the working-side mandible were at their peak. At this time, EMG activity has peaked in the working- and balancing-side superficial masseters, anterior temporales, and medial pterygoids, as well as in the working-side posterior temporalis, and is decreasing in amplitude. In contrast, EMG amplitudes in the balancing-side deep masseter and posterior temporalis are at their peak (SOM Fig. S1).

Hylander et al. (1987) reported that late activity in the balancing-side deep masseter was accompanied by decreased activity in the balancing-side medial pterygoid and increasing activity

in the working-side medial pterygoid. They hypothesized that this combination of muscle forces resulted in large lateral transverse bending moments on the mandible, producing wishboning of the symphyseal region late in the power stroke (Hylander, 1984; Hylander et al., 1987). In contrast, our EMG data show that both medial pterygoids display decreasing EMG activity at the time when the balancing-side deep masseter is showing peak activity. Consequently, when our data are used to calculate the moments acting on the mandible, the loading regime on the balancing-side corpus is dominated by sagittal shear forces and sagittal bending moments (Figs. 3C and 4F, G); lateral transverse bending moments are comparatively low. The balancing-side corpus does experience negative AP—twisting—moments, but these torques are relatively

Maximum difference across food types

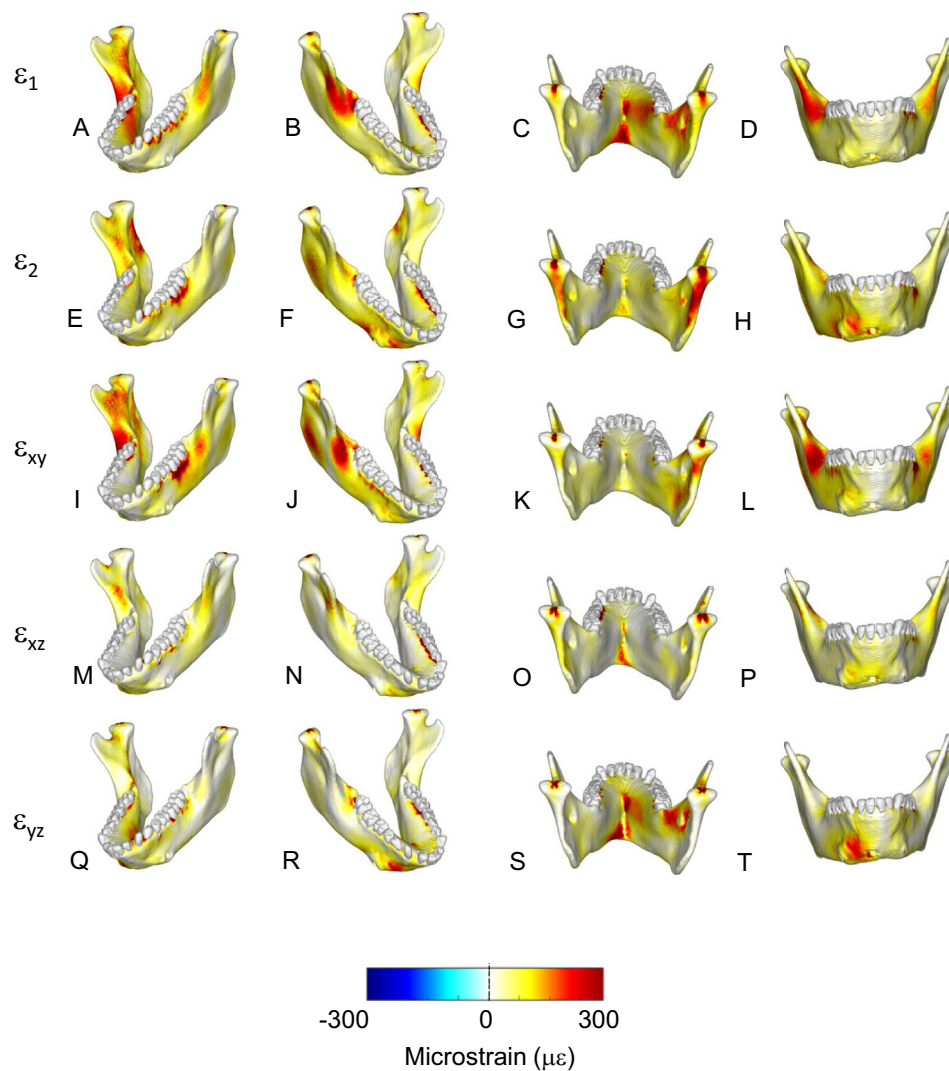


Figure 10. Comparisons of maximum differences in magnitudes of strain components from simulations of mastication of all food types. Figures map the distribution of the maximum differences in principal (A–H) and shear (I–T) strains recorded on the surfaces of the model during simulation of the power stroke of mastication on any of the three foods. The top two rows present principal strains; the bottom three rows present shear strains. The scale bar at the bottom indicates the difference in microstrain ($\mu\epsilon$).

low everywhere except in the anterior corpus. In the corpus under the premolars, lateral transverse bending moments and AP twisting moments reach their highest values, approaching the sagittal bending moments in magnitude, which are low in this region of the mandible (Fig. 2).

On the working side, the AP twisting moments and lateral transverse bending are similar in magnitude to those on the balancing side, but the sagittal bending moments are lower. Sagittal bending moments, AP twisting moments, and lateral transverse bending moments all reach similar maxima in the corpus below the bite points (P_3 , P_4 , and M_1), and lateral transverse shear forces also peak in the anterior corpus. At progressively more posterior sections through the working-side corpus, sagittal bending moments decrease more rapidly than AP torques, so that they are roughly equal in magnitude in the region of M_2 , and AP torques are larger than transverse or vertical torques in the corpus below M_3 . Sagittal shear is the dominant loading regime behind the bite point (Figs. 2 and 3B). Hylander (1979c) suggested that biting on the anterior

region of the postcanine tooth row (as modeled here) would generate negative AP torques—inverting the base of the mandible—under the bite point and that muscle forces would generate positive AP torques—everting the base and angle of the ramus. Our loading and deformation regimes corroborate this hypothesis (Fig. 2; SOM Fig. S6). Examination of the individual torques acting about a frontal section through the mandible below M_1 confirms that bite force contributes significantly to negative AP twisting moments acting on the working-side postcanine corpus. It also reveals powerful negative AP twisting moments generated by vertical components of balancing-side muscle force, previously neglected in discussions of primate mandibular mechanics. The largest negative twisting moments are associated with the vertical and horizontal components of bite force acting on M_1 and the vertical components of balancing-side temporalis and superficial masseter muscle force (Table 2).

Importantly, our modeling provides new insight into the loading regime of the symphyseal region late in the power

Maximum effects on principal strain orientations

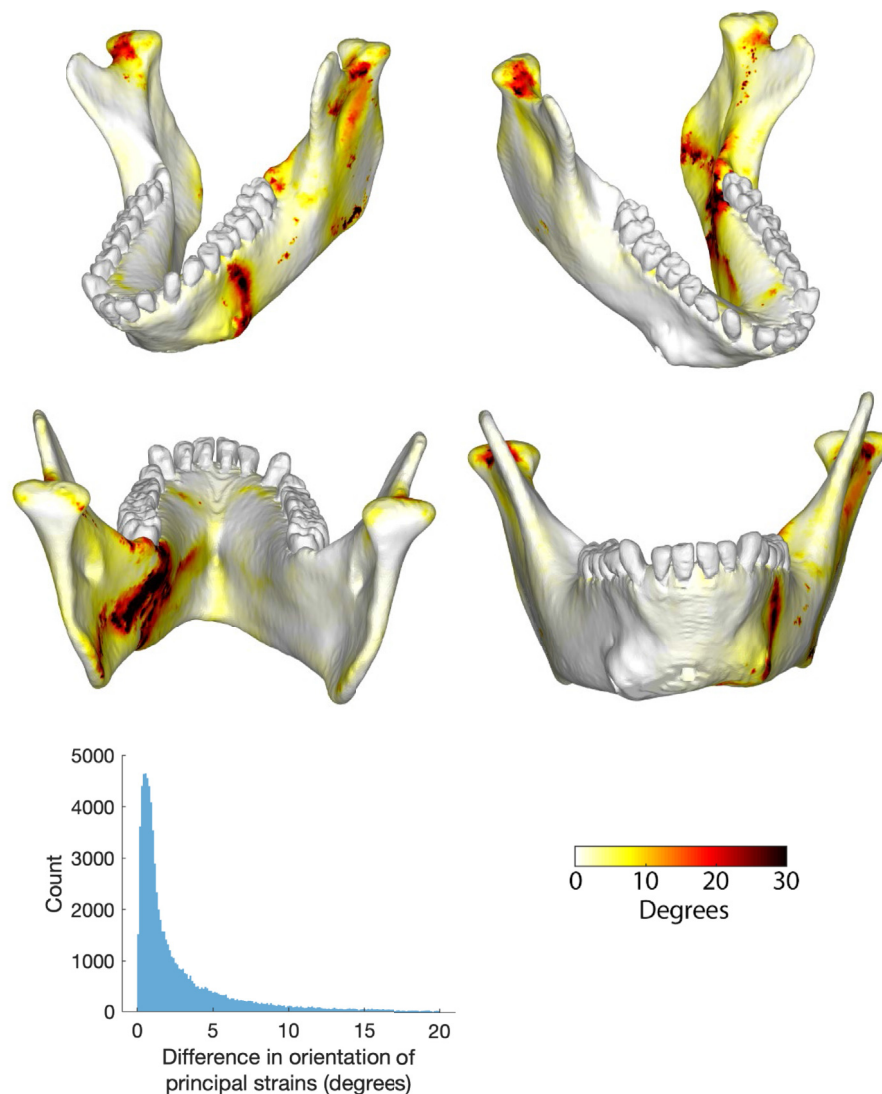


Figure 11. Comparisons of differences in orientation of principal strains from simulations of mastication of the three food types. Figures map the distribution of the differences in principal strain orientations recorded on the surfaces of the model during simulation of the power stroke of mastication on nuts and dried fruit. The scale bar at the bottom indicates the difference in degrees. Histogram shows number of elements with given differences in principal strain orientations.

stroke. In vivo bone strain recordings from the labial surface of the symphyseal region in macaques suggest that negative frontal shear and/or negative ML twisting are important loading regimes in the symphyseal region (Hylander, 1984). However, it was not possible to discriminate between these loading regimes using in vivo data because it is difficult to record strain from the lingual aspect of the symphyseal region during normal feeding (Hylander, 1979b) and because information on the moments acting about the symphysis has been scant. Our estimates of the loading regime in the symphysis confirm the presence of large negative shearing forces (-30 N) in frontal planes through the symphyseal region (Fig. 3), and our strain data do reveal negative frontal shear strains on the labial surface of the symphysis (Fig. 6). However, analysis of all the moments acting about the symphyseal region reveals that at this time in the power stroke, negative ML twisting moments (0.7 Nm) are greater than AP twisting moments (0.4 Nm) and approach lateral transverse bending (wishboning) moments (1.0 Nm) in magnitude (Figs. 2

and 6I–K). The combination of negative AP twisting of both working- and balancing-side mandibles means that the center of flexure of frontal bending of the symphyseal region is not in the midline (Beecher, 1977; Demes et al., 1984; Wolff, 1984), but is shifted toward the working side (Korioth and Hannam, 1994; Korioth et al., 1992). Moreover, negative AP twisting of both working- and balancing-side mandibles means that positive frontal shear strain is an important component of symphyseal loading. In sum, the symphyseal region does experience the hypothesized positive frontal bending, albeit with a different center of flexure, and the predominant loading regimes are lateral transverse bending and negative ML twisting.

4.2. Strain regimes

The strain regime in the balancing-side mandible reflects the superposition of sagittal and lateral transverse bending. Tensile AP and ϵ_1 strains dominate the top of the balancing-side corpus and

most of the lingual/medial surface of the corpus and ramus, especially the medial prominence and endocondylar ridge (Figs. 4H, I and 6B), whereas compressive AP and ϵ_2 strains dominate the lateral/buccal surface of the balancing-side mandible, especially its base (Fig. 4J–L). Negative AP twisting is associated with positive transverse shear strains in the medial prominence, extramolar sulcus, and endocondylar ridge and with negative transverse shear strains in the base of the mandible. High sagittal shearing forces are associated with high-magnitude sagittal shear strains on the lateral surface of the balancing-side mandible, at the corpus-ramus junction (extramolar sulcus, external oblique line), and in the ramus in and above the endocondylar ridge.

The strain regime in the working-side mandible is marked by strain magnitudes that are, on average, lower than strain magnitudes on the balancing side. As on the balancing side, sagittal shear strains are high in the buccal surface and reflect changing patterns of shear forces (Fig. 5F, G). Sagittal bending is associated with alternating patches of positive and negative AP and principal strains in the alveolar process and mandibular base; similar alternating patches of transverse shear strains are associated with alternating patterns of torsion (Fig. 5C, D). Alternating patches of tension and compression have been shown to characterize the base of FEM of human and *Alligator* mandibles under unilateral loading (Korioth et al., 1992; Rudderman and Mullen, 1992) and are hypothesized for opossums on the basis of in vivo strain gauge studies (Crompton, 1995). Alternating patterns of shear strain in the basal surface associated with alternating twisting moments have not previously been observed. Our in vivo strain gauge data and strain data from the surface of our model below the posterior tooth row (Panagiotopoulou et al., 2017) are similar to those reported by Hylander (1979c, 1981) from the buccal (summarized in Ross et al., 2016: Fig. 1) and lingual surfaces of the working-side corpus (Dechow and Hylander, 2000): ϵ_1 is oriented upward and backward on the buccal surface and upward and forward on the lingual surface.

In the symphyseal region, lateral transverse bending results in high-magnitude ϵ_1 and transverse shear strains lingually and high ϵ_2 strains labially (Fig. 6B, D, F). However, the combination of lateral transverse bending and negative ML twisting means that these strains are not evenly distributed across the symphyseal region. In association with negative ML twisting, the symphyseal region experiences high-magnitude frontal and transverse shear strains of opposite signs in lingual and labial surfaces, strains which reach their peaks in the superior and inferior transverse tori (Fig. 6I–K).

The inaccessibility of the ramus for in vivo strain gauge recordings means it has been neglected in most recent work on primate mandible biomechanics; our modeling results suggest that more attention to the ramus is warranted. Our estimates of loading regimes reveal high-magnitude shearing forces and moments acting on the rami, and strain magnitudes are also high in some regions of the rami. Both working- and balancing-side rami experience high-magnitude ϵ_1 strains on the front edges, and high ϵ_2 on the back edges of the rami associated with the high-magnitude negative sagittal bending moments acting in those coronal planes. On the balancing side, ϵ_2 strain magnitudes in the back edge of the ramus are higher than those on the working side because reaction forces from the temporomandibular joint are higher on the balancing side. High-strain magnitudes are also apparent in the endocondylar ridge and torus triangularis on the medial surface of the balancing-side ramus, including high-magnitude AP tensile and ϵ_1 strains associated with negative sagittal bending, transverse tensile and shear strains associated with lateral transverse bending, and positive transverse shear strains associated with negative AP torsion (Fig. 4C, H, I). These fields of high-magnitude strains in the endocondylar ridge and torus triangularis are posterior

continuations of fields of similarly high strains in the lingual face and upper edge of the corpus. We hypothesize that these fields of high-magnitude strain extending from the bite point to the balancing-side condyle constitute the primary load path, with the torus triangularis and the endocondylar ridge constituting the load path across the ramus.

In modern engineering parlance, the load path is the combination of part(s) of a complex structure—usually the stiffest route—that transfers the majority of the load (force) from the load point (bite point) to the support points (condyles). External ridges of cortical bone and internal ‘trajectories’ of trabecular bone have long been argued to be important pathways for transmission of forces through the mandible, whether from the muscle to bite point or from the muscle and bite point to the temporomandibular joint (TMJ; Gaspard, 1978; Lenhossek, 1920; Walkhoff, 1902; Weidenreich, 1936). Lenhossek (1920) argued that the external oblique line and the torus triangularis reinforce the ramus and transfer temporalis muscle force to the alveolar process and teeth. Weidenreich (1936: 65–66) proposed that the endocondylar ridge and external oblique lines are “means of transmission of force issuing from the coronoid and condyloid processes” to the corpus and that the endocoronoid ridge and endocondylar crest are “beams strengthening the bone in that direction on which the strain and force is transmitted from both processes to the body of the jaw.” Weidenreich (1936) further hypothesized that the crista ectocondyloidea performed a similar function on the lateral surface of the ramus. Our modeling reveals that the endocondylar ridge, torus triangularis, and external oblique lines are highly strained, suggesting that they do transmit large forces. Thus, one key finding from this study is that the morphology of these features may be informative about strain regimes in the anthropoid mandible during mastication. The same cannot be said for the ectocondyloid crest, which does not experience high strains. This crest likely owes its existence to resorption and thinning of bone in planum triangulare lateralis, rather than to reinforcement for transmission of force. In this regard, it is worth noting that the ectocondyloid crest lies below the level of the endocondylar ridge and therefore does not correspond to the ridge’s lateral surface.

It is of interest to compare this concentrated strip of high strain in the macaque mandible with the absence of such paths in crania of primates. As we have discussed elsewhere (Prado et al., 2016), the theory of ‘pillars and buttresses’ in the primate cranium is, with the exception of the anterior pillar, not supported by the available morphological and strain data. The only place where a functional pillar—a strip of highly strained bone extending from the tooth row toward the calvaria—is observed is the anterior pillar in macaques, chimpanzees, and some fossil humans (Prado et al., 2016).

4.3. Impact of food mechanical properties and relevance for hominid evolutionary studies

Comparative morphometric studies of the relationship between mandible morphology, feeding behavior, and diet have used measures of corpus and symphyseal morphology with limited success (Daegling, 1990, 1992, 2007b; Daegling and Grine, 1991, 2006; Daegling and McGraw, 2000, 2001, 2007; Daegling et al., 2011; Hylander, 1988; Ravosa, 1991, 2000; Ross and Iriarte-Diaz, 2014, 2019; Taylor, 2002, 2006a, b). Our modeling suggests possible reasons for this. One measure used to make inferences about diet is corpus depth, a measure of resistance to sagittal bending. Under sagittal bending, the principal and axial strains should be highest in the upper and lower surfaces of the mandible; to decrease these strains, all things being equal, the depth of the mandible should be increased. Our analysis confirms that late in the power stroke, sagittal bending moments are high on both working and balancing

sides (higher than both AP twisting and transverse bending moments; Fig. 2), and principal and AP axial strains are high in upper and lower surfaces of the mandible (Fig. 4). Moreover, of all the moments acting on the balancing-side corpus, sagittal bending moments show the largest interfood differences: nut chewing is associated with higher sagittal bending moments than either dried fruit or grape chewing (Fig. 7). Therefore, it is noteworthy that the largest interfood differences in AP axial and principal strains are not uniformly seen in the upper and lower surfaces of the corpus (Figs. 9 and 10). Instead, the largest differences in ϵ_1 are seen in a strip running along the medial prominence, across the extramolar sulcus to the external oblique line, and along the medial surface of the endocondylar ridge. If mandible form was to be modified to ameliorate these food-related differences in strain magnitudes, it is not obvious that increases in corpus depth would be the most efficient solution. Adding cortical bone to the inferior border to deepen the corpus would certainly increase the resistance to sagittal bending, decreasing strains in the upper and lower surfaces of the corpus, but this is not where food-related variation in strain magnitudes is greatest. Moreover, if food-related changes in corpus shape were effected by recruiting plasticity mechanisms that use strain magnitude as a trigger (Frost, 2003, 2004), our results suggest these mechanisms would not result in increases in corpus depth, but, rather, increases in size or density of the medial prominence and endocondylar ridge.

The external forces producing sagittal bending moments in the balancing- and working-side mandibles also result in large sagittal shearing forces. These are associated with high-magnitude sagittal shear strains in the corpus-ramus junction—recessus mandibulae, extramolar sulcus, external oblique line—on both working and balancing sides, as well as the buccal faces of both corpora (behind the bite point on the working side; Fig. 4; SOM Fig. S5A–E). These same areas display some of the largest food effects on sagittal shear strains (Fig. 9). To increase resistance to these food-related increases in sagittal shearing forces, there is no special advantage to increasing corpus depth to increase resistance to increased sagittal shear; rather, cortical bone thickness can be increased anywhere in frontal sections, but especially in locations where cortical bone thickness is reduced. Measures of cortical bone distribution below M₁ and M₂ in the corpus in several groups of primates reveal no significant differences in the relative contribution of the cortical bone area to the subperiosteal area between extant and fossil hominids, between three species of cercopithecoids with different diets, or between *Cebus capucinus* and *Sapajus apella* (Daegling, 1989, 1992, 2002). Based on our loading and strain results, we hypothesize that estimates of cortical bone area at more posterior sections, where shear strains are also high, might yield stronger dietary signals.

Another external measure frequently used to make dietary inferences is corpus breadth, roughly in frontal planes, a measure of resistance to transverse bending and, under some mechanical models, torsion (Daegling and Hylander, 1998). Under lateral transverse bending, high-magnitude axial and principal strains in the medial and lateral surfaces can be reduced by increasing beam thickness in transverse planes. High-magnitude transverse shear strains can be resisted by increasing the amount of bone in frontal cross sections. In our model, lateral transverse bending of the balancing-side mandible is indeed associated with high-magnitude AP tensile and ϵ_1 strains along the lingual surface of the corpus, high-magnitude AP compressive and ϵ_2 strains along the buccal surface, and positive transverse shear strain in the medial prominence and endocondylar ridge (Fig. 6B, D). However, as noted previously, the greatest interfood variation in ϵ_1 is seen in a strip along the lingual surface of the corpus, a strip that lies within the region characterized by high-magnitude ϵ_1 : medial prominence,

extramolar sulcus, torus triangularis, and endocondylar ridge (Fig. 10A–D). Moreover, food-related differences in loading regimes are associated with increased lateral transverse bending moments, especially anteriorly in the corpus (Fig. 7). If mandible form was to be modified to ameliorate these food-related differences in strain magnitudes, adding cortical bone to the medial prominence would simultaneously increase resistance to transverse bending and reduce strains in highly strained areas. Moreover, if food-related changes in corpus shape were affected by recruiting plasticity mechanisms that use strain magnitude as a trigger (Frost, 2003, 2004), our results suggest these mechanisms would result in increases in size or density of the extramolar sulcus, torus triangularis, and endocondylar ridge.

Corpus breadth is also one of several measures used to estimate the resistance of the corpus to AP twisting or torsion, the other measures including Bredt's formula (Daegling, 1989, 1992, 2002, 2007a; Daegling and Hylander, 1998). It is sometimes assumed that chewing on foods of increased dietary toughness or hardness results in increased torsional stress in the corpus associated with increases in the lateral components of jaw elevator muscle force and bite force (Bouvier, 1986a, b; Daegling, 1989; Daegling and Grine, 1991; Hylander, 1988; Ravosa, 1991, 1996a, b, 1999, 2000; Taylor, 2002, 2006a, b; Taylor et al., 2008). In our study, the largest differences in loading and strain regimes (Figs. 7 and 9) are between nuts (characterized by relatively low toughness and high stiffness) on the one hand and grapes (relatively low toughness and stiffness) and dried fruits (relatively high toughness and low stiffness) on the other hand. It is noteworthy that AP twisting moments show the lowest differences between foods, especially in the posterior corpus (Fig. 7). Many fossil hominids have very broad corpora under the molars, and this has been interpreted as improving resistance to torsional stresses associated with eating tougher, harder foods (Daegling, 1989, 1990, 1992, 2001; Daegling and Grine, 1991, 2006; Hylander, 1988). Our macaque data do not support the hypothesis that increased dietary toughness explains the broad corpora of fossil hominids. We acknowledge that the foods fed to our experimental animals are not the most mechanically challenging foods eaten by primates in the laboratory (Williams et al., 2005) or in the wild (Coiner-Collier et al., 2016; Dominy et al., 2008; McGraw et al., 2011, 2014; Vogel et al., 2008; Wright, 2005; Yamashita, 2008), and macaque occlusal morphology differs from that of fossil hominids. Thus, it is possible that our findings for macaques are species specific. Studies in other primate species relating variation in muscle activity during chewing on different foods to variation in mandibular strain regimes are needed to confirm the differences in interfood loading regimes observed in this study. As noted elsewhere, posterior displacement of the tooth row relative to the anterior border of the ramus in hominids necessitates broadening of the mandible at the ramus-corpus junction regardless of dietary factors (Daegling and Grine, 1991). Our results suggest that interactions between spatial, dietary, and mechanical factors in this highly strained part of the mandible may be of interest in future studies of hominid feeding adaptations.

In the symphyseal region, variables used to infer diet include measures of the distribution of cortical bone, as well as maximum and minimum dimensions, the mechanical meanings of which vary with the orientation of the symphysis (Daegling, 1992, 2001; Ravosa, 2000). In the macaque modeled here, as in many cercopithecine monkeys, the maximum dimension from the tooth row (symphysis or infradentale anterior) to the back of the inferior transverse torus is oriented obliquely (at about 45°) to the plane of the postcanine tooth rows. This means that, as in hominids, a large proportion of the symphyseal cross section is oriented so as to reduce moments and strains associated with transverse bending (Daegling, 2001). Interpreting the mechanical significance of

interspecific variation in these measures is complicated by the difficulty of estimating the moments and shear forces acting on the symphyseal region. Our modeling reveals similar magnitudes of food-related variation in AP, SI, and ML moments, with the largest differences being in SI—lateral transverse bending—moments (Fig. 7). Our FEM study confirms that the lingual surfaces of the superior and the inferior transverse tori experience the highest ML tensile strains and the highest ε_1 strains, as expected for the concave surfaces of a curved symphyseal region under lateral transverse bending (Hylander, 1984; Fig. 6). Moreover, there is significant food-related variation in ε_1 strain in the posterior surfaces of the superior and (especially) the inferior transverse tori (Figs. 9 and 10). Thus, our empirical findings support the frequent theoretical assumption that measures of symphyseal resistance to lateral transverse bending are good candidates for recovering dietary signals in fossil hominid mandibles. However, lateral transverse bending is not the only important loading regime in the symphyseal region: our modeling results suggest that the ML twisting regime also results in transverse and frontal shear strains on lingual/labial or superior/inferior surfaces of the symphyseal region that equal or exceed those associated with lateral transverse bending (Fig. 6). Food-related variation in ML twisting moments is less than that of lateral transverse bending (Fig. 6), but food-related variation in transverse shear strains in the symphyseal region is significant (Fig. 9Q–T). These results suggest that symphyseal measures that capture resistance to ML twisting, notably the distribution of cortical bone in the symphyseal region, may also be useful for dietary reconstruction in fossil taxa.

One of the most interesting results of our modeling is the observation that these areas of the symphyseal region that experience high-magnitude ε_1 and transverse shear strains are continuous with similar areas along the balancing-side mandible—medial prominence, retromolar triangle, extramolar sulcus, torus triangularis, and endocondylar ridge. We suggested previously that this strain distribution might indicate that this is the principal load path from the bite point to the balancing-side condyle. In this context, it is significant that these areas, from the symphysis to endocondylar ridge, also manifest the largest variation in maximum principal and transverse shear strain magnitudes, both of which increase in nut chewing compared with dried fruit and grape chewing. With the exception of the superior transverse torus in the symphyseal region, traditional external morphometric measures do not capture variation in morphology in these parts of the mandible. Recent experimental (Ravosa et al., 2007; Terhune et al., 2020) and comparative studies (Coiner-Collier et al., 2018; Giesen et al., 2003a, b, 2004; Giesen and van Eijden, 2000) relating internal morphology of the symphysis and condyle to variation in food material properties suggest that work elsewhere along the load path might be of value. However, optimism that this work will reveal highly specific indicators of feeding on specific foods should be tempered by the fact that the load path does not manifest food-specific variation in principal strain orientation: ε_1 orientation in these areas is largely unaffected by chewing on different foods (Fig. 11). The largest changes in principal strain orientations are instead concentrated under the medial and alveolar prominences and on the front of the condylar neck on the working side, areas where food-associated variation in strain magnitudes is negligible. Nevertheless, variation in cortical bone distribution and in trabecular size and number (if not orientation) along the load path may also provide information on dietary habits.

The broader relevance of this study, including studies of human evolutionary biomechanics, rests in part on similarities between the loading regime documented here and loading regimes acting on other primate mandibles. Our EMG data document late activity in the balancing-side deep masseter and posterior

temporalis, simultaneous with decreasing activity in medial pterygoids and superficial masseters (SOM Fig. S1). A triplet motor pattern is seen late in the power stroke in approximately 54% of chewing cycles by *Macaca fuscata* and 73% of chewing cycles by *Papio anubis* (see Ram and Ross, 2018) and has been described for humans (Langenbach and Hannam, 1999; Møller, 1966) and *Pan*, albeit at a lower frequency (Ram and Ross, 2018). Our model also resembles finite element models of the human mandible in patterns of deformation—rotation about the bite point, eversion of the balancing-side and inversion of the working-side mandible base—and strain, including AP compressive strains in the alveolar process and AP tensile strains in the base of the mandible under the bite point (Korioth and Versluis, 1997; Rudderman and Mullen, 1992; van Eijden, 2000). This suggests that the results presented here may be relevant to hypotheses of mandible function during a significant proportion of cercopithecine and some hominid chewing cycles. In particular, morphological measures of resistance to lateral transverse bending may provide dietary information, as might detailed studies of trabecular morphology in the transverse tori, medial prominence, torus triangularis, and endocondylar ridge.

5. Conclusions

Musculoskeletal modeling and FEM of the macaque mandible during mastication suggest that the most important loading regimes in balancing and working hemimandibles are sagittal bending, sagittal shear, and lateral transverse bending, with AP twisting moments being smaller. The largest food-related variation in corpus loading regimes is in sagittal bending and shear; food-related variation in lateral transverse bending is highest in the anterior corpus: food-related variation in AP twisting of the corpora is minimal. In the symphyseal region, lateral transverse bending and negative ML twisting are important loading regimes, and both show high levels of food-related variation. Food-related variation in strain regimes is greatest in the lingual symphysis, in the balancing-side corpus-ramus junction, and along the balancing-side medial prominence and endocondylar ridge. This includes some areas of traditional focus—lingual symphysis—and areas that have not previously been considered. Specifically, our work highlights the importance of the medial prominence, torus triangularis, and endocondylar ridge and suggests that these may constitute the load path from the bite point to the balancing-side condyle and ramus.

Conflict of interest

The authors have no competing interests.

Acknowledgments

The authors acknowledge the following: Marie Curie European Re-integration Grant ERG-MACACA 267207 to O.P.; CIHR Grant MOP-4918, the National Institutes of Health (NIH RO1DE023816), Brain Research Foundation to C.F.R.; and National Science Foundation (BCS0962677) and an NIH (R24 HD050837-01) grant to A.B.T. The authors thank the editors and reviewers for their help with this paper.

Supplementary Online Material

Supplementary Online Material to this article can be found online at <https://doi.org/10.1016/j.jhevol.2020.102865>.

References

- Anapol, F., Shahnoor, N., Ross, C.F., 2008. Scaling of reduced physiological cross-sectional area in primate muscles of mastication. In: Vinyard, C., Wall, C.E., Ravosa, M.J. (Eds.), *Primate Craniofacial Function and Biology*. Springer, New York, pp. 201–216.
- Beecher, R.M., 1977. Function and fusion at the mandibular symphysis. *Am. J. Phys. Anthropol.* 47, 325–336.
- Bouvier, M., 1986a. A biomechanical analysis of mandibular scaling in Old World monkeys. *Am. J. Phys. Anthropol.* 69, 473–482.
- Bouvier, M., 1986b. Biomechanical scaling of mandibular dimensions in New World monkeys. *Int. J. Primatol.* 7, 551–567.
- Chalk, J., Richmond, B.G., Ross, C.F., Strait, D.S., Wright, B.W., Spencer, M.A., Wang, Q., Dechow, P.C., 2011. A finite element analysis of masticatory stress hypotheses. *Am. J. Phys. Anthropol.* 145, 1–10.
- Coiner-Collier, S., Scott, R.S., Chalk-Wilayto, J., Cheyne, S.M., Constantino, P., Dominy, N.J., Elgart, A.A., Glowacka, H., Loyola, L.C., Ossi-Lupo, K., Raguett-Schofield, M., Talebi, M.G., Sala, E.A., Sieradzy, P., Taylor, A.B., Vinyard, C.J., Wright, B.W., Yamashita, N., Lucas, P.W., Vogel, E.R., 2016. Primate dietary ecology in the context of food mechanical properties. *J. Hum. Evol.* 98, 103–118.
- Coiner-Collier, S., Vogel, E.R., Scott, R.S., 2018. Trabecular anisotropy in the primate mandibular condyle is associated with dietary toughness. *Anat. Rec.* 301, 1342–1359.
- Crompton, A.W., 1995. Masticatory function in nonmammalian cynodonts and early mammals. In: Thomason, J.J. (Ed.), *Functional Morphology in Vertebrate Paleontology*. Cambridge University Press, New York, pp. 55–75.
- Daegling, D.J., 1989. Biomechanics of cross-sectional size and shape in the hominoid mandibular corpus. *Am. J. Phys. Anthropol.* 80, 91–106.
- Daegling, D.J., 1990. Geometry and biomechanics of hominoid mandibles. Ph.D. Dissertation, State University of New York at Stony Brook.
- Daegling, D.J., 1992. Mandibular morphology and diet in the genus *Cebus*. *Int. J. Primatol.* 13, 545–570.
- Daegling, D.J., 1993. The relationship of in vivo bone strain to mandibular corpus morphology in *Macaca fascicularis*. *J. Hum. Evol.* 25, 247–269.
- Daegling, D.J., 2001. Biomechanical scaling of the hominoid mandibular symphysis. *J. Morphol.* 250, 12–23.
- Daegling, D.J., 2002. Bone geometry in cercopithecoid mandibles. *Arch. Oral Biol.* 47, 315–325.
- Daegling, D.J., 2007a. Morphometric estimation of torsional stiffness and strength in primate mandibles. *Am. J. Phys. Anthropol.* 132, 261–266.
- Daegling, D.J., 2007b. Relationship of bone utilization and biomechanical competence in hominoid mandibles. *Arch. Oral Biol.* 52, 51–63.
- Daegling, D.J., Carlson, K.J., Tafforeau, P., de Ruiter, D.J., Berger, L.R., 2016. Comparative biomechanics of *Australopithecus sediba* mandibles. *J. Hum. Evol.* 100, 73–86.
- Daegling, D.J., Grine, F.E., 1991. Compact bone distribution and biomechanics of early hominid mandibles. *Am. J. Phys. Anthropol.* 86, 321–339.
- Daegling, D.J., Grine, F.E., 2006. Mandibular biomechanics and the paleontological evidence for the evolution of human diet. In: Ungar, P.S. (Ed.), *Evolution of the Human Diet: The Known, the Unknown, and the Unknowable*. Oxford University Press, Cary, pp. 77–105.
- Daegling, D.J., Hotzman, J., 2003. Functional significance of cortical bone distribution in anthropoid mandibles: An in vitro assessment of bone strain under combined loads. *Am. J. Phys. Anthropol.* 122, 38–50.
- Daegling, D.J., Hylander, W.L., 1998. Biomechanics of torsion in the human mandible. *Am. J. Phys. Anthropol.* 105, 73–87.
- Daegling, D.J., Hylander, W.L., 2000. Experimental observation, theoretical models, and biomechanical inference in the study of mandibular form. *Am. J. Phys. Anthropol.* 112, 541–551.
- Daegling, D.J., McGraw, W.S., 2000. Gnathic morphology and feeding ecology in papionin primates. *Am. J. Phys. Anthropol.* 111 (S30), 134.
- Daegling, D.J., McGraw, W.S., 2001. Feeding, diet, and jaw form in West African *Colobus* and *Procolobus*. *Int. J. Primatol.* 22, 1033–1055.
- Daegling, D.J., McGraw, W.S., 2007. Functional morphology of the mangabey mandibular corpus: Relationship to dental specializations and feeding behavior. *Am. J. Phys. Anthropol.* 134, 50–62.
- Daegling, D.J., McGraw, W.S., Ungar, P.S., Pampush, J.D., Vick, A.E., Bitty, E.A., 2011. Hard-object feeding in sooty mangabeys (*Cercocebus atys*) and interpretation of early hominin feeding ecology. *PLoS One* 6, e23095.
- Daegling, D.J., Ravosa, M.J., Johnson, K.R., Hylander, W.L., 1992. Influence of teeth, alveoli, and periodontal ligaments on torsional rigidity in human mandibles. *Am. J. Phys. Anthropol.* 89, 59–72.
- Dechow, P.C., Hylander, W.L., 2000. Elastic properties and masticatory bone stress in the macaque mandible. *Am. J. Phys. Anthropol.* 112, 541–552.
- Dechow, P.C., Panagiotopoulou, O., Gharpure, P., 2017. Biomechanical implications of cortical elastic properties of the macaque mandible. *Zoology (Jena)* 124, 3–12.
- Demes, B., Preuschoft, H., Wolff, J.E.A., 1984. Stress-strength relationship in the mandible of hominoids. In: Chivers, D., Wood, B., Bilsborough, A. (Eds.), *Food Acquisition and Processing in Primates*. Plenum Press, New York, pp. 369–390.
- Dominy, N.J., Vogel, E.R., Yeakel, J.D., Constantino, P., Lucas, P.W., 2008. Mechanical properties of plant underground storage organs and implications for dietary models of early hominins. *Evol. Biol.* 35, 159–175.
- Felder, A., Ward, S.R., Lieber, R.L., 2005. Sarcomere length measurement permits high resolution normalization of muscle fiber lengths in architectural studies. *J. Exp. Biol.* 208, 3275–3279.
- Frost, H.M., 2003. Bone's mechanostat: a 2003 update. *Anat. Rec.* 275, 1081–1101.
- Frost, H.M., 2004. A 2003 update of bone physiology and Wolff's Law for clinicians. *Angle Orthod.* 74, 3–15.
- Gaspard, M., 1978. L'Appareil Manducateur et la Manducation. Anatomie Descriptive, Ontogenèse et Phylogenèse de la Mandibule Humaine. Première Partie, Volume 1. J. Prélât, Paris.
- Giesen, E.B., Ding, M., Dalstra, M., van Eijden, T.M., 2003a. Architectural measures of the cancellous bone of the mandibular condyle identified by principal components analysis. *Calcif. Tissue Int.* 73, 225–231.
- Giesen, E.B., Ding, M., Dalstra, M., van Eijden, T.M., 2003b. Reduced mechanical load decreases the density, stiffness, and strength of cancellous bone of the mandibular condyle. *Clin. Biomech.* 18, 358–363.
- Giesen, E.B., Ding, M., Dalstra, M., van Eijden, T.M., 2004. Changed morphology and mechanical properties of cancellous bone in the mandibular condyles of edentate people. *J. Dent. Res.* 83, 255–259.
- Giesen, E.B., van Eijden, T.M., 2000. The three-dimensional cancellous bone architecture of the human mandibular condyle. *J. Dent. Res.* 79, 957–963.
- Grine, F.E., Judex, S., Daegling, D.J., Ozcivici, E., Ungar, P.S., Teaford, M.F., Sponheimer, M., Scott, J., Scott, R.S., Walker, A., 2010. Craniofacial biomechanics and functional and dietary inferences in hominin paleontology. *J. Hum. Evol.* 58, 293–308.
- Gröning, F., Fagan, M., O'Higgins, P., 2012. Modeling the human mandible under masticatory loads: which input variables are important? *Anat. Rec.* 295, 853–863.
- Hibbeler, R.C., 2000. *Mechanics of Materials*. Prentice Hall, Upper Saddle River, New Jersey.
- Hylander, W.L., 1977. In vivo bone strain in the mandible of *Galago crassicaudatus*. *Am. J. Phys. Anthropol.* 46, 309–326.
- Hylander, W.L., 1979a. An experimental analysis of temporomandibular joint reaction force in macaques. *Am. J. Phys. Anthropol.* 51, 433–456.
- Hylander, W.L., 1979b. The functional significance of primate mandibular form. *J. Morphol.* 160, 223–240.
- Hylander, W.L., 1979c. Mandibular function in *Galago crassicaudatus* and *Macaca fascicularis*: An in vivo approach to stress analysis of the mandible. *J. Morphol.* 159, 253–296.
- Hylander, W.L., 1981. Patterns of stress and strain in the macaque mandible. In: Carlson, D.S. (Ed.), *Craniofacial Biology*. University of Michigan, Ann Arbor, pp. 1–35.
- Hylander, W.L., 1984. Stress and strain in the mandibular symphysis of primates: A test of competing hypotheses. *Am. J. Phys. Anthropol.* 64, 1–46.
- Hylander, W.L., 1985. Mandibular function and biomechanical stress and scaling. *Am. Zool.* 25, 315–330.
- Hylander, W.L., 1986. In vivo bone strain as an indicator of masticatory bite force in *Macaca fascicularis*. *Arch. Oral Biol.* 31, 149–157.
- Hylander, W.L., 1988. Implications of in vivo experiments for interpreting the functional significance of "robust" australopithecine jaws. In: Grine, F.E. (Ed.), *Evolutionary History of the "Robust" Australopithecines*. Aldine de Gruyter, New York, pp. 55–83.
- Hylander, W.L., Crompton, A.W., 1986. Jaw movements and patterns of mandibular bone strain during mastication in the monkey *Macaca fascicularis*. *Arch. Oral Biol.* 31, 841–848.
- Hylander, W.L., Johnson, K.R., 1989. The relationship between masseter force and masseter electromyogram during mastication in the monkey *Macaca fascicularis*. *Arch. Oral Biol.* 34, 713–722.
- Hylander, W.L., Johnson, K.R., 1993. Modeling relative masseter force from surface electromyograms during mastication in non-human primates. *Arch. Oral Biol.* 38, 233–240.
- Hylander, W.L., Johnson, K.R., 1994. Jaw muscle function and wishboning of the mandible during mastication in macaques and baboons. *Am. J. Phys. Anthropol.* 94, 523–547.
- Hylander, W.L., Johnson, K.R., 1997. In vivo bone strain patterns in the zygomatic arch of macaques and the significance of these patterns for functional interpretations of craniofacial form. *Am. J. Phys. Anthropol.* 102, 203–232.
- Hylander, W.L., Johnson, K.R., Crompton, A.W., 1987. Loading patterns and jaw movements during mastication in *Macaca fascicularis*: A bone-strain, electromyographic, and cineradiographic analysis. *Am. J. Phys. Anthropol.* 72, 287–314.
- Hylander, W.L., Picq, P.G., Johnson, K.R., 1991. Masticatory-stress hypotheses and the supraorbital region of primates. *Am. J. Phys. Anthropol.* 86, 1–36.
- Hylander, W.L., Ravosa, M.J., Ross, C.F., 2004. Jaw muscle recruitment patterns during mastication in anthropoids and prosimians. In: Anapol, F., German, R.Z., Jablonski, N.G. (Eds.), *Shaping Primate Evolution*. Cambridge University Press, Cambridge, pp. 229–257.
- Hylander, W.L., Ravosa, M.J., Ross, C.F., Johnson, K.R., 1998. Mandibular corpus strain in Primates: Further evidence for a functional link between symphyseal fusion and jaw-adductor muscle force. *Am. J. Phys. Anthropol.* 107, 257–271.
- Hylander, W.L., Ravosa, M.J., Ross, C.F., Wall, C.E., Johnson, K.R., 2000. Symphyseal fusion and jaw-adductor muscle force: An EMG study. *Am. J. Phys. Anthropol.* 112, 469–492.
- Hylander, W.L., Vinyard, C.J., Wall, C.E., Williams, S.H., Johnson, K.R., 2002. Recruitment and firing patterns of jaw muscles during mastication in ring-tailed lemurs. *Am. J. Phys. Anthropol.* 117 (S34), 88.
- Hylander, W.L., Vinyard, C.J., Wall, C.E., Williams, S.H., Johnson, K.R., 2011. Functional and evolutionary significance of the recruitment and firing patterns of the jaw

- adductors during chewing in verreaux's sifaka (*Propithecus verreauxi*). *Am. J. Phys. Anthropol.* 145, 531–547.
- Hylander, W.L., Wall, C.E., Vinyard, C.J., Ross, C., Ravosa, M.R., Williams, S.H., Johnson, K.R., 2005. Temporalis function in anthropoids and strepsirrhines: An EMG study. *Am. J. Phys. Anthropol.* 128, 35–56.
- Keiter, F., 1935. An anthropological study of the Schwabische Alb Mountain Range Region. *Petermanns Mitt.* 81, 254.
- Korioth, T.W., Hannam, A.G., 1994. Deformation of the human mandible during simulated tooth clenching. *J. Dent. Res.* 73, 56–66.
- Korioth, T.W., Romilly, D.P., Hannam, A.G., 1992. Three-dimensional finite element stress analysis of the dentate human mandible. *Am. J. Phys. Anthropol.* 88, 69–96.
- Korioth, T.W., Versluis, A., 1997. Modeling the mechanical behavior of the jaws and their related structures by finite element (FE) analysis. *Crit. Rev. Oral Biol. Med.* 8, 90–104.
- Langenbach, G.E.J., Hannam, A.G., 1999. The role of passive muscle tensions in a three-dimensional dynamic model of the human jaw. *Arch. Oral Biol.* 44, 557–573.
- Ledogar, J.A., Smith, A.L., Benazzi, S., Weber, G.W., Spencer, M.A., Carlson, K.B., McNulty, K.P., Dechow, P.C., Grosse, I.R., Ross, C.F., Richmond, B.G., Wright, B.W., Wang, Q., Byron, C., Carlson, K.J., de Ruiter, D.J., Berger, L.R., Tamvada, K., Pryor, L.C., Berthaume, M.A., Strait, D.S., 2016. Mechanical evidence that *Australopithecus sediba* was limited in its ability to eat hard foods. *Nat. Commun.* 7, 10596.
- Lenhossek, M.v., 1920. Das innere Relief des Unterkieferastens. *Arch. Anthropol.* 18, 49–59.
- Lieberman, D.E., Ross, C.F., Ravosa, M.J., 2000. The primate cranial base: ontogeny, function, and integration. *Yearbk. Phys. Anthropol.* 43, 117–169.
- McGraw, W.S., Daegling, D.J., 2012. Primate feeding and foraging: Integrating studies of behavior and morphology. *Annu. Rev. Anthropol.* 41, 203–219.
- McGraw, W.S., Daegling, D.J., 2020. Diet, feeding behavior, and jaw architecture of Tai monkeys: Congruence and chaos in the realm of functional morphology. *Evol. Anthropol.* 29, 14–28.
- McGraw, W.S., Vick, A.E., Daegling, D.J., 2011. Sex and age differences in the diet and ingestive behaviors of sooty mangabeys (*Cercocebus atys*) in the Tai Forest, Ivory Coast. *Am. J. Phys. Anthropol.* 144, 140–153.
- McGraw, W.S., Vick, A.E., Daegling, D.J., 2014. Dietary variation and food hardness in sooty mangabeys (*Cercocebus atys*): Implications for fallback foods and dental adaptation. *Am. J. Phys. Anthropol.* 154, 413–423.
- Mehari Abraha, H., Iriarte-Diaz, J., Ross, C.F., Taylor, A.B., Panagiotopoulou, O., 2019. The mechanical effect of the periodontal ligament on bone strain regimes in a validated finite element model of a macaque mandible. *Front. Bioeng. Biotech.* 7, 269.
- Mendez, J., Keys, A., 1960. Density and composition of mammalian muscle. *Metabolism* 9, 184–188.
- Møller, E., 1966. The chewing apparatus. An electromyographic study of the action of the muscles of mastication and its correlation to facial morphology. *Acta Physiol. Scand.* 69 (Suppl. 280), 1–229.
- Moazen, M., Curtis, N., O'Higgins, P., Evans, S.E., Fagan, M.J., 2009. Biomechanical assessment of evolutionary changes in the lepidosaurian skull. *Proc. Natl. Acad. Sci. USA* 106, 8273–8277.
- Panagiotopoulou, O., Iriarte-Diaz, J., Wilshin, S., Dechow, P.C., Taylor, A.B., Mehari Abraha, H., Aljunid, S.F., Ross, C.F., 2017. In vivo bone strain and finite element modeling of a rhesus macaque mandible during mastication. *Zoology* 124, 13–29.
- Piveteau, J., 1957. *Traité de Paléontologie*, vol. 7. *Primates: Paléontologie Humaine*, Masson, Paris.
- Porro, L.B., Holliday, C.M., Anapol, F., Ontiveros, L.C., Ontiveros, L.T., Ross, C.F., 2011. Free body analysis, beam mechanics, and finite element modeling of the mandible of *Alligator mississippiensis*. *J. Morphol.* 272, 910–937.
- Porro, L.B., Metzger, K., Iriarte-Diaz, J., Ross, C.F., 2013. In vivo bone strain and finite element modeling of the mandible of *Alligator mississippiensis*. *J. Anat.* 223, 195–227.
- Prado, F.B., Freire, A.R., Claudia Rossi, A., Ledogar, J.A., Smith, A.L., Dechow, P.C., Strait, D.S., Voigt, T., Ross, C.F., 2016. Review of in vivo bone strain studies and finite element models of the zygomatic complex in humans and nonhuman primates: Implications for clinical research and practice. *Anat. Rec.* 299, 1753–1778.
- Rak, Y., 1983. *The Australopithecine Face*. Academic Press, New York.
- Ram, Y., Ross, C.F., 2018. Evaluating the triplet hypothesis during rhythmic mastication in Primates. *J. Exp. Biol.* 221, jeb165985.
- Rasche, W., 1913. Beiträge zur Anthropologie des Unterkiefers. *Kgl. Hof- und Univ.-Buchdr. Dr. C. Wolf & Sohn, München*.
- Ravosa, M.J., 1988. Browridge development in Cercopithecidae: A test of two models. *Am. J. Phys. Anthropol.* 76, 535–555.
- Ravosa, M.J., 1991. Structural allometry of the mandibular corpus and symphysis in prosimian primates. *J. Hum. Evol.* 20, 3–20.
- Ravosa, M.J., 1996a. Jaw morphology and function in living and fossil Old World Monkeys. *Int. J. Primatol.* 17, 909–932.
- Ravosa, M.J., 1996b. Mandibular form and function in North American and European Adapidae and Omomyidae. *J. Morphol.* 229, 171–190.
- Ravosa, M.J., 1999. Anthropoid origins and the modern symphysis. *Folia Primatol.* 70, 65–78.
- Ravosa, M.J., 2000. Size and scaling in the mandible of living and extinct apes. *Folia Primatol.* 71, 305–322.
- Ravosa, M.J., Hogue, A., 2004. Function and fusion of the mandibular symphysis in mammals: a comparative and experimental perspective. In: Ross, C.F., Kay, R.F. (Eds.), *Anthropoid Origins: New Visions*. Kluwer Academic/Plenum Publishers, New York, pp. 413–462.
- Ravosa, M.J., Kunwar, R., Stock, S.R., Stack, M.S., 2007. Pushing the limit: masticatory stress and adaptive plasticity in mammalian craniomandibular joints. *J. Exp. Biol.* 210, 628–641.
- Ravosa, M.J., Menegaz, R.A., Scott, J.E., Daegling, D.J., McAbee, K.R., 2016. Limitations of a morphological criterion of adaptive inference in the fossil record. *Biol. Rev.* 91, 883–898.
- Ravosa, M.J., Simons, E.L., 1994. Mandibular growth and function in *Archaeolemur*. *Am. J. Phys. Anthropol.* 95, 63–76.
- Ravosa, M.J., Vinyard, C.J., Gagnon, M., Islam, S.A., 2000. Evolution of anthropoid jaw loading and kinematic patterns. *Am. J. Phys. Anthropol.* 112, 493–516.
- Rayfield, E.J., 2011. Strain in the ostrich mandible during simulated pecking and validation of specimen-specific finite element models. *J. Anat.* 218, 47–58.
- Reed, D.A., Ross, C.F., 2010. The influence of food material properties on jaw kinematics in the primate, *Cebus*. *Arch. Oral Biol.* 55, 946–962.
- Rightmire, G.P., Deacon, H.J., 1991. Comparative studies of Late Pleistocene human remains from Klasies River Mouth, South Africa. *J. Hum. Evol.* 20, 131–156.
- Robinson, J.T., 1972. *Early Hominid Posture and Locomotion*. University of Chicago Press, Chicago.
- Ross, C.F., Berthaume, M.A., Dechow, P.C., Iriarte-Diaz, J., Porro, L.B., Richmond, B.G., Spencer, M., Strait, D., 2011. In vivo bone strain and finite-element modeling of the craniofacial haft in catarrhine primates. *J. Anat.* 218, 112–148.
- Ross, C.F., Iriarte-Diaz, J., 2014. What does feeding system morphology tell us about feeding? *Evol. Anthropol.* 23, 105–120.
- Ross, C.F., Iriarte-Diaz, J., 2019. Evolution, constraint and optimality in primate feeding systems. In: Bels, V., Whishaw, I.Q. (Eds.), *Feeding in Vertebrates*. Springer, Cham, pp. 787–828.
- Ross, C.F., Iriarte-Diaz, J., Nunn, C.L., 2012. Innovative approaches to the relationship between diet and mandibular morphology in primates. *Int. J. Primatol.* 33, 632–660.
- Ross, C.F., Iriarte-Diaz, J., Reed, D.A., Stewart, T.A., Taylor, T.B., 2016. In vivo bone strain in the mandibular corpus of *Sapajus* during a range of oral food processing behaviors. *J. Hum. Evol.* 98, 36–65.
- Ross, C.F., Washington, R.L., Eckhardt, A., Reed, D.A., Vogel, E.R., Dominy, N.J., Machanda, Z.P., 2009. Ecological consequences of scaling of chew cycle duration and daily feeding time in Primates. *J. Hum. Evol.* 56, 570–585.
- Rudderman, R.H., Mullen, R.L., 1992. Biomechanics of the facial skeleton. *Clin. Plast. Surg.* 19, 11–29.
- Scott, R.S., Ungar, P.S., Bergstrom, T.S., Brown, C.A., Grine, F.E., Teaford, M.F., Walker, A., 2005. Dental microwear texture analysis shows within-species diet variability in fossil hominins. *Nature* 436, 693–695.
- Shahnoor, S., 2004. Morphological adaptations to diet in primate masticatory muscles. Ph.D. Dissertation, University of Wisconsin-Milwaukee.
- Sinclair, A.G., Alexander, R.M., 1987. Estimated forces exerted by the jaw muscles of some reptiles. *J. Zool.* 213, 107–115.
- Smith, A.L., Benazzi, S., Ledogar, J.A., Tamvada, K., Pryor Smith, L.C., Weber, G.W., Spencer, M.A., Dechow, P.C., Grosse, I.R., Ross, C.F., Richmond, B.G., Wright, B.W., Wang, Q., Byron, C., Slice, D.E., Strait, D.S., 2015a. Biomechanical implications of intraspecific shape variation in chimpanzee crania: moving toward an integration of geometric morphometrics and finite element analysis. *Anat. Rec.* 298, 122–144.
- Smith, A.L., Benazzi, S., Ledogar, J.A., Tamvada, K., Pryor Smith, L.C., Weber, G.W., Spencer, M.A., Lucas, P.W., Michael, S., Shekeban, A., Al-Fadhalah, K., Almusallam, A.S., Dechow, P.C., Grosse, I.R., Ross, C.F., Madden, R.H., Richmond, B.G., Wright, B.W., Wang, Q., Byron, C., Slice, D.E., Wood, S., Dzialo, C., Berthaume, M.A., van Casteren, A., Strait, D.S., 2015b. The feeding biomechanics and dietary ecology of *Paranthropus boisei*. *Anat. Rec.* 298, 145–167.
- Spears, I.R., Macho, G.A., 1998. Biomechanical behaviour of modern human molars: Implications for interpreting the fossil record. *Am. J. Phys. Anthropol.* 106, 467–482.
- Strait, D.S., Constantino, P., Lucas, P.W., Richmond, B.G., Spencer, M.A., Dechow, P.C., Ross, C.F., Grosse, I.R., Wright, B.W., Wood, B.A., Weber, G.W., Wang, Q., Byron, C., Slice, D.E., Chalk, J., Smith, A.L., Smith, L.C., Wood, S., Berthaume, M., Benazzi, S., Dzialo, C., Tamvada, K., Ledogar, J.A., 2013. Viewpoints: diet and dietary adaptations in early hominins: the hard food perspective. *Am. J. Phys. Anthropol.* 151, 339–355.
- Strait, D.S., Grosse, I.R., Dechow, P.C., Smith, A.L., Wang, Q., Weber, G.W., Neubauer, S., Slice, D.E., Chalk, J., Richmond, B.G., Lucas, P.W., Spencer, M.A., Schrein, C., Wright, B.W., Byron, C.D., Ross, C.F., 2010. The structural rigidity of the cranium of *Australopithecus africanus*: Implications for diet, dietary adaptations, and the allometry of feeding biomechanics. *Anat. Rec.* 293, 583–593.
- Strait, D., Richmond, B.G., Spencer, M., Ross, C.F., Wood, B., 2007. Something to chew on: Masticatory biomechanics and its relevance to early hominid phylogeny. *J. Hum. Evol.* 52, 585–599.
- Strait, D., Wang, Q., Dechow, P.C., Ross, C.F., Richmond, B., Spencer, M., Patel, B.A., 2005. Modeling elastic properties in finite element analysis: how much precision is needed to produce an accurate model? *Anat. Rec.* 283A, 275–287.
- Strait, D.S., Weber, G.W., Neubauer, S., Chalk, J., Richmond, B.G., Lucas, P.W., Spencer, M.A., Schrein, C., Dechow, P.C., Ross, C.F., Grosse, I.R., Wright, B.W., Constantino, P., Wood, B.A., Lawn, B., Hylander, W.L., Wang, Q., Byron, C.,

- Slice, D.E., Smith, A.L., 2009. The feeding biomechanics and dietary ecology of *Australopithecus africanus*. *Proc. Natl. Acad. Sci. USA* 106, 2124–2129.
- Taylor, A.B., 2002. Masticatory form and function in the African apes. *Am. J. Phys. Anthropol.* 117, 133–156.
- Taylor, A.B., 2005. A comparative analysis of temporomandibular joint morphology in the African apes. *J. Hum. Evol.* 48, 555–574.
- Taylor, A.B., 2006a. Diet and mandibular morphology in African apes. *Int. J. Primatol.* 27, 181–201.
- Taylor, A.B., 2006b. Feeding behavior, diet, and the functional consequences of jaw form in orangutans, with implications for the evolution of *Pongo*. *J. Hum. Evol.* 50, 377–393.
- Taylor, A.B., Eng, C.M., Anapol, F.C., Vinyard, C.J., 2009. The functional correlates of jaw-muscle fiber architecture in tree-gouging and nongouging callitrichid monkeys. *Am. J. Phys. Anthropol.* 139, 353–367.
- Taylor, A.B., Vinyard, C.J., 2009. Jaw-muscle fiber architecture in tufted capuchins favors generating relatively large muscle forces without compromising jaw gape. *J. Hum. Evol.* 57, 710–720.
- Taylor, A.B., Vinyard, C.J., 2013. The relationships among jaw-muscle fiber architecture, jaw morphology and feeding behavior in extant apes and modern humans. *Am. J. Phys. Anthropol.* 151, 120–134.
- Taylor, A.B., Vogel, E.R., Dominy, N.J., 2008. Food material properties and mandibular load resistance abilities in large-bodied hominoids. *J. Hum. Evol.* 55, 604–616.
- Taylor, A.B., Yuan, T., Ross, C.F., Vinyard, C.J., 2015. Jaw-muscle force and excursion scale with negative allometry in platyrrhine primates. *Am. J. Phys. Anthropol.* 158, 242–256.
- Terhune, C.E., Sylvester, A.D., Scott, J.E., Ravosa, M.J., 2020. Internal architecture of the mandibular condyle of rabbits is related to dietary resistance during growth. *J. Exp. Biol.* <https://doi.org/10.1242/jeb.220988>.
- Ungar, P.S., Grine, F.E., Teaford, M.F., 2008. Dental microwear and diet of the Pliocene hominin *Paranthropus boisei*. *PLoS One* 3, e2044.
- van Eijden, T.M., 2000. Biomechanics of the mandible. *Crit. Rev. Oral Biol. Med.* 11, 123–136.
- Vinyard, C.J., Ravosa, M.J., 1998. Ontogeny, function, and scaling of the mandibular symphysis in papionin primates. *J. Morphol.* 235, 157–175.
- Virchow, H., 1916. Zahnbogen und Alveolarbogen. *Z. Ethnol.* 48, 277–295.
- Virchow, H., 1920. Die menschlichen Skeletreste aus dem Kämpfe'schen Bruch im Travertin von Ehringsdorf bei Weimar. Verlag von Gustav Fischer, Jena.
- Vogel, E.R., van Woerden, J.T., Lucas, P.W., Atmoko, S.S.U., van Schaik, C.P., Dominy, N.J., 2008. Functional ecology and evolution of hominoid molar enamel thickness: *Pan troglodytes schweinfurthii* and *Pongo pygmaeus wurmbii*. *J. Hum. Evol.* 55, 60–74.
- Vogel, E.R., Zulfa, A., Hardus, M.E., Wich, S.A., Dominy, N.J., Taylor, A.B., 2014. Food mechanical properties, feeding ecology, and the mandibular morphology of wild orangutans. *J. Hum. Evol.* 75, 110–124.
- Walkhoff, O., 1902. Der Unterkiefer des Anthropomorphen und des Menschen in seiner funktionellen Entwicklung und Gestalt. C. W. Kreidel's Verlag, Wiesbaden.
- Weidenreich, F., 1936. The mandibles of *Sinanthropus pekinensis*: A comparative study. *Palaeontol. Sinica* 7, 1–162.
- Weijjs, W.A., 1980. Biomechanical models and the analysis of form: a study of the mammalian masticatory apparatus. *Am. Zool.* 20, 707–719.
- Weijjs, W.A., Dantuma, R., 1975. Electromyography and mechanics of mastication in the albino rat. *J. Morphol.* 146, 1–34.
- Weijjs, W.A., Dantuma, R., 1981. Functional anatomy of the masticatory apparatus in the rabbit (*Oryctolagus cuniculus* L.). *Neth. J. Zool.* 31, 99–147.
- Weijjs, W.A., Van der Wielen-Drent, T.K., 1982. Sarcomere length and EMG activity in some jaw muscles of the rabbit. *Acta Anat.* 113, 178–188.
- Weijjs, W.A., Van Ruijven, L.J., 1990. Models of masticatory mechanics: Their reliability, resolving power and usefulness in functional morphology. *Neth. J. Zool.* 40, 136–152.
- White, T.D., Black, M.T., Folkens, P.A., 2012. Skull: Cranium and Mandible. In: White, T.D., Black, M.T., Folkens, P.A. (Eds.), *Human Osteology*, 3rd ed. Academic Press, San Diego, pp. 43–100.
- Williams, S.H., Wright, B.W., Truong, V., Daubert, C.R., Vinyard, C.J., 2005. Mechanical properties of foods used in experimental studies of primate masticatory function. *Am. J. Primatol.* 67, 329–346.
- Wolff, J.E.A., 1984. A theoretical approach to solve the chin problem. In: Chivers, D., Wood, B., Bilsborough, A. (Eds.), *Food Acquisition and Processing in Primates*. Plenum, New York, pp. 391–405.
- Wolpoff, M.H., 1980. *Paleoanthropology*. Alfred A. Knopf, New York.
- Wright, B.W., 2005. Craniodental biomechanics and dietary toughness in the genus *Cebus*. *J. Hum. Evol.* 48, 473–492.
- Wroe, S., Moreno, K., Clausen, P., McHenry, C., Curnoe, D., 2007. High-resolution three-dimensional computer simulation of hominid cranial mechanics. *Anat. Rec.* 290, 1248–1255.
- Yamashita, N., 2008. Food physical properties and their relationship to morphology: The curious case of *kily*. In: Vinyard, C., Ravosa, M.J., Wall, C.E. (Eds.), *Primate Craniofacial Function and Biology*. Springer, New York, pp. 387–406.